Huhmann BL, Neumann A, Boyanov MI, Kemner KM, Scherer MM.
As(V) in Magnetite: Incorporation and Redistribution.
***Environmental Science: Processes and Impacts* (2017)**
DOI: https://doi.org/10.1039/C7EM00237H

As(V) in Magnetite: Incorporation and Redistribution

Brittany L. Huhmann[1,2#], Anke Neumann[3#], Maxim I. Boyanov[4,5], Kenneth M. Kemner[4], and Michelle M. Scherer[1]*

[1]Department of Civil and Environmental Engineering, University of Iowa, Iowa City, IA, 52242, United States

[2]*Present Address:* Department of Civil and Environmental Engineering, Massachusetts Institute of Technology, Cambridge, MA, 02139, United States

[3]School of Engineering, Newcastle University, Newcastle upon Tyne, NE1 7RU, United Kingdom

[4]Biosciences Division, Argonne National Laboratory, Argonne, IL, 60439, United States

[5]Institute of Chemical Engineering, Bulgarian Academy of Sciences, Sofia 1113, Bulgaria

[#]*Author Contributions:* Brittany Huhmann and Anke Neumann contributed equally to this work.

[*]*Corresponding Author:* phone: +44 191 208 6406; email: anke.neumann@ncl.ac.uk

Submitted to: *Environmental Science: Processes and Impact*.

Environmental impact statement

We present evidence that coprecipitation with magnetite can sequester a high proportion of dissolved As(V) into the magnetite structure. Once incorporated into magnetite, As(V) could not be remobilized, neither in the absence nor in the presence of aqueous Fe(II), suggesting that magnetite is a stable sink for As(V). We also found that As(V) sorbed to pre-formed magnetite, in both the absence and presence of aqueous Fe(II), became increasingly incorporated over time and thus resistant to remobilization. Our results increase our understanding of how Fe minerals affect As mobility in natural systems. In addition, our results provide molecular-level insight needed for the development of iron oxide-based As removal technologies.

Abstract

Exposure to As in groundwater negatively impacts millions of people around the globe, and As mobility in groundwater is often controlled by Fe mineral dissolution and precipitation. Additionally, trace elements can be released from and incorporated into the structure of Fe oxides in the presence of dissolved Fe(II). The potential for As to redistribute between sorbed on the magnetite surface and incorporated in the magnetite structure, however, remains

unclear. In this study, we use selective chemical extraction and X-ray absorption spectroscopy (XAS) to distinguish magnetite-sorbed and incorporated As(V) and to provide evidence for As(V) incorporation during magnetite precipitation. While As in the As-magnetite coprecipitates did not redistribute between sorbed and incorporated over a 4 month period, a small, but measurable increase in incorporated As(V) of up to 13% was observed for sorbed As(V). We suggest that Fe(II)-catalyzed recrystallization of magnetite did not significantly influence the redistribution of sorbed As(V) because the extent of Fe atom exchange was small (~10%). In addition, the extent of As redistribution was the same in the absence and presence of added aqueous Fe(II), suggesting that aqueous Fe(II) had, overall, a minor effect on As redistribution for both coprecipitated and sorbed As(V). Our results suggest that coprecipitation of As(V) with magnetite and redistribution of As(V) sorbed on magnetite are potential pathways for irreversible As(V) uptake and sequestration. These pathways are likely to play a significant role in controlling As mobility in natural systems, during human-induced redox cycling of groundwater such as aquifer storage and recovery, as well as in iron oxide-based As removal systems.

Introduction

Geologic As contamination of groundwater is a concern in many regions of the world, where the use of As-contaminated water as a drinking water source is threatening human health. In addition, As-contaminated groundwater in these regions is often used for crop irrigation, which can result in As uptake by crops and decreases in crop yields, thus posing a threat to food security.[1, 2] In Bangladesh alone, tens of millions of people have been exposed to As[3] and have been affected by As poisoning.[4]

Iron redox chemistry plays a key role in the environmental cycling of many elements, including As. Iron is the element which most strongly correlates with As in sediments, and As mobilization is frequently linked with the desorption/dissolution of As from iron oxides.[5] Additionally, As removal from drinking water, for example using electrocoagulation or zero-valent iron based filters, relies on the sequestration of As with Fe oxides,[6-8] which might, in analogy to As mobilization in reducing aquifers, release some or all of the sequestered As over time. Although many different Fe oxides may form in the environment, only magnetite has been identified as an important sink for As in recent remediation approaches[9], drinking water treatment systems[10], and natural sediments.[11] It is thus critical to better understand how magnetite, which was the predominant Fe oxide phase associated with As in iron-based filters in Bangladesh, remained the stable sink for As for time periods extending over several years.[10]

Under reducing conditions, such as those found in groundwater in As-affected regions, aqueous Fe(II) is widely present and can interact with Fe oxides. In the presence of aqueous Fe(II), unstable Fe oxides such as lepidocrocite and ferrihydrite can transform to more stable Fe oxides such as magnetite and goethite[12, 13] and stable Fe oxides can incorporate and release other elements. For example, Ni and Zn are released from goethite and hematite[14] and Mn is released from goethite[15] in the presence of Fe(II). Furthermore, incorporation of Ni into hematite[16] and Tc(IV) into goethite[17] in the presence of Fe(II) has been suggested based on X-ray absorption spectroscopy (XAS) data. In contrast, XAS data suggest that As(V)

remained sorbed or precipitated as ferrous arsenate rather than being incorporated into goethite or hematite in the presence of Fe(II).[18] Structural incorporation of As(V), however, has been found to occur during magnetite precipitation,[19, 20] and during the reductive transformation of lepidocrocite and 2-line ferrihydrite to magnetite.[20-22] It is currently unknown whether As, once incorporated into magnetite, remains stably bound within the magnetite structure or becomes remobilized as sorbed or aqueous As in the presence of aqueous Fe(II). Similarly, it is unclear whether As(V) sorbed to magnetite remains sorbed or can become redistributed over time. Recent work demonstrated that measurable dynamic Fe atom exchange occurs when magnetite is exposed to aqueous Fe(II),[23, 24] which suggests the possibility for concomitant As(V) incorporation into the magnetite structure.

In this study, we investigated the potential for As(V) incorporation into magnetite by coprecipitating magnetite with As(V) as well as reacting As(V) with pre-formed magnetite in the absence and presence of added Fe(II). We then validated and used sodium hydroxide extractions to distinguish between sorbed and incorporated As(V) and X-ray absorption spectroscopy to determine the As binding environment. In addition, we tested whether redistribution of sorbed and coprecipitated As(V) in our experiments was linked to previously observed Fe(II)-catalyzed magnetite recrystallization[23] by measuring the extent of Fe atom exchange in ^{57}Fe isotope enriched tracer experiments.

Materials and Methods

All experiments were carried out in an anaerobic chamber (N_2/H_2 of 93/7) with residual oxygen concentrations below 1 ppm. Solutions were purged with N_2 for at least 2 h prior to transfer into the anaerobic chamber. Before use in any experimental procedure, solutions, glassware, plastics, and solids were equilibrated within the anaerobic chamber overnight.

Mineral Synthesis and Characterization

Magnetite batches were synthesized in an anaerobic chamber as previously described.[25] Briefly, isotopically-normal Fe(II) and Fe(III) were combined at a 1:2 ratio in deionized water (added as $FeCl_2$ and $FeCl_3 \cdot 6H_2O$, respectively) before raising the solution pH to 10-11 with NaOH. Magnetite precipitates were aged in anoxic suspension for 24 hours. For As-coprecipitated magnetite, As(V) was added before the pH was raised to begin magnetite precipitation, similar to the method described in Wang *et al*.[20] Initial As:Fe mole ratios were between 0.001 and 0.01, which fall within the range of As:Fe ratios reported for naturally occurring Fe oxides (i.e., 2.4×10^{-6} to 9.0×10^{-2})[3, 26, 27], and final As:Fe mole ratios measured by dissolution were 0.0005 and 0.0099. After synthesis, the magnetite was ground and sieved through a 150 micron sieve. XRD samples were prepared by mixing magnetite solids with a small amount of glycerol to prevent oxidation during the measurement. Magnetite was the only phase detected using pXRD (**Figure S1**). The stoichiometry of each batch was determined by dissolving pre-weighed samples in 5 M HCl in an anaerobic glovebox.[28] Fe(II) and total Fe were measured colorimetrically using the 1,10-phenanthroline method, as previously described.[25, 28] Mineral synthesis and characterization parameters can be found in **Table S1**.

As(V) Extraction

An extraction protocol based on the high efficiency of hydroxide to desorb As(V) from Fe oxides[29, 30] was adopted to differentiate between surface-bound and incorporated As(V) following precipitation of magnetite in the presence of As(V) and reaction of magnetite with As(V) in the presence and absence of aqueous Fe(II). To extract the sorbed As(V), 15 mg of magnetite was added to 15 mL of 1 M NaOH (giving a solid concentration of 1 g/L) in triplicate 30 mL Oak Ridge style centrifuge tube reactors. The reactors were allowed to react for 4 hours in the dark on a rotator in the anaerobic chamber. After the reaction, the centrifuge tubes were sealed with an O-ring and Teflon tape. The reactors were centrifuged outside the glovebox at 13,000 × g for 15 min and immediately returned to the glovebox. The supernatant was decanted off the pelleted magnetite and filtered through a 0.22 μm filter. This was followed by a second, 20-hour extraction with 1 M NaOH, and the solution was again centrifuged and the aqueous phase decanted. The remaining solids were dissolved in 5 mL of 5 M HCl.

Total Fe was measured by the 1,10-phenanthroline method[31, 32] and showed that less than 1% of the Fe was extracted by the NaOH (data not shown). As(V) concentrations were measured on a Thermo Fisher Scientific X Series 2 Quadrupole Inductively Coupled Plasma-Mass Spectrometer (ICP-MS) with a glass concentric nebulizer and a HEPA filtered autosampler. The ICP-MS was operated in collision cell mode using 7% H_2, 93% He (>99.996% pure) as collision cell gas with a flow rate of 4 mL min^{-1} to remove isobaric interferences. Specific isobaric interferences ($^{40}Ar^{35}Cl$ with ^{75}As) were monitored and generally low, and were corrected as suggested elsewhere.[33, 34] An internal standard (10 ppb of ^{89}Y) was used to correct instrument drift.

Batch experiments

Reactors were assembled in 30 mL Oak Ridge style centrifuge tubes and were allowed to react in the dark on a rotator in the anaerobic chamber. All experiments were conducted in triplicate, unless otherwise indicated.

Adsorption isotherm of As(V) on magnetite

An adsorption isotherm was constructed to determine when surface saturation was reached for As adsorption on magnetite at a pH value of 7.2. For each data point (single reactors), 15 mg of magnetite was added to 15 mL of 50 mM non-complexing MOPS (3-(N-morpholino)propanesulfonic acid, pKa 7.20[35]) buffer adjusted to pH 7.2 and was allowed to equilibrate for 24 hours, followed by As(V) addition at defined concentrations between 10 and 1000 μM. After 24 hours, the reactors were centrifuged and the aqueous phase was decanted, filtered (0.22 μm nylon filter), and acidified with 50 μL of concentrated HCl. Arsenic concentrations in the aqueous phase were measured by ICP-MS, as described above.

Sorption of As(V) to magnetite in the presence and absence of Fe(II)

As(V) sorption to magnetite in the presence and absence of Fe(II) was monitored over time spans ranging from 30 minutes to 124 days. Reactors contained 15 mg magnetite pre-equilibrated in 15 mL of 50 mM non-complexing MOPS buffer (pH 7.2) for 24 hours and 13.3 μM of As. The As concentration used in our experiment is 100-fold greater than the EPA's drinking water standard of 0.133 μM, yet it is within the range of As concentrations observed in natural waters (>0.01 μM to <66.74 μM) und thus of environmental relevance.[5]

For selected reactors, 1 mM Fe(II) was added after equilibration with As (5 hours) and the pH was adjusted to 7.2. After predetermined time intervals, the reactors were centrifuged at 13,000 × g for 15 min and the supernatant was decanted off the pelleted magnetite, filtered (0.22 μm nylon filter), and acidified. The magnetite was subjected to the NaOH extraction described above. Arsenic concentrations in all phases were measured by ICP-MS.

Redistribution of As in magnetite coprecipitates in the presence and absence of Fe(II)

Similar to the sorption experiments but in the absence of added aqueous As(V), As distribution in As-magnetite coprecipitates in the presence and absence of Fe(II) was monitored over time spans ranging from 5 to 123 days. Reactors comprised 15 mg of magnetite coprecipitated with As (As:Fe mole ratio of 0.01; freeze-dried, ground, and sieved), 15 mL of 50 mM non-complexing MOPS buffer (pH 7.2), and, for selected reactors, 1 mM Fe(II) that was added after overnight equilibration. Centrifugation, extraction, and sample preparation and analysis were identical to the sorption experiments.

Batch experiments for XAS analysis

For XAS analysis of As(V) associated with magnetite, sorption experiments were conducted at a higher As(V) concentration of 2936 μM As(V) and a higher mass loading of 150 mg magnetite, with all other conditions identical to the experimental setup described above. Experiments were run for 30 minutes to almost 8 days and were carried out in sextuplet reactors, which were split equally for subsequent XAS analysis and As(V) extraction. For XAS analysis, the magnetite from the three designated reactors was combined prior to analysis.

X-ray Absorption Spectroscopy

The oxidation state and binding environment of As in our samples was determined by using As K-edge (11,867 eV) x-ray absorption spectroscopy (XAS), which was carried out at the MR-CAT/EnviroCAT insertion device beamline (Sector 10, Advanced Photon Source).[36] Fluorescence-mode x-ray absorption near edge spectra (XANES) and extended x-ray absorption fine structure (EXAFS) spectra were collected from the adsorption and co-precipitation samples using an Ar-filled ionization chamber. The magnetite solids were separated by filtration through a 0.22 μm PTFE filter inside an anoxic glove box (Coy technologies, 5% H_2/balance N_2, Pd catalyst, O_2 in the gas environment <1 ppm at all times) and the hydrated filter cake was sealed together with the membrane between sheets of Kapton film. Reference minerals scorodite and symplesite as well as the sorption samples run for 30 minutes and in the presence of added aqueous Fe(II) were dried over desiccant in the glovebox and measured as powders packed in a holder. Spectra were collected at room temperature inside a N_2-purged sample cell. Anoxic integrity of samples prepared this way have been demonstrated in previous work.[37] Energy calibration was established by collecting a spectrum from a Au foil and setting the inflection point at 11,919 eV. Calibration was maintained continuously afterwards by measurements of spectra from a stable As reference (As_2O_3) simultaneously with the collection of data from the samples. Radiation-induced changes in the speciation of As were not observed in quick XANES scans (<30 sec each) on a fresh area of the samples. No differences were observed between spectra collected from

several different areas on the sample so all scans were combined to produce the final spectrum from each sample.

Analysis of the experimental spectra involved comparisons to As standards followed by structural modeling of the data to extract the structural parameters describing the average atomic coordination around As. Standards included polycrystalline scorodite ($FeAsO_4 \cdot 2H_2O$), polycrystalline symplesite ($Fe^{II}_3(AsO_4)2 \bullet 8(H_2O)$) (both verified by p-XRD, **Figure S1**), dissolved As(V) (10 mM AsO_4^{3-} solution at pH 7), and polycrystalline As_2O_3 as the As(III) standard (obtained from Sigma-Aldrich). The polycrystalline As powders were mounted on the adhesive side of Kapton tape and their absorption spectra were measured in transmission mode. The solution standard was mounted in a 1.5 mm thick sample holder with Kapton windows and the spectrum was measured in fluorescence. Normalization and background removal of the data was accomplished using the program AUTOBK.[38] The structural analyses of the spectra are based on the crystal structure of scorodite. [39] The code FEFF8 [40] was used to generate the single-scattering contributions in the EXAFS for the O and Fe coordination shells in scorodite. Refinement of the structural parameters against the experimental data was done in R-space using the program FEFFIT.[41]

Iron Atom Exchange Experiments

To determine the extent of Fe(II)-catalyzed magnetite recrystallization in the presence of sorbed and coprecipitated As(V), we carried out isotope exchange experiments using aqueous Fe(II) enriched in the ^{57}Fe isotope. This approach has been applied to magnetite previously and is documented in detail elsewhere.[23] In short, 15 mg magnetite with Fe in its natural isotope composition were exposed to 1 mM $^{57}Fe(II)$ in 15 mL of 50 mM non-complexing MOPS buffer (pH 7.2). After 10 min to 7 days reaction time, the triplicate reactors were centrifuged and the aqueous phase decanted, filtered (0.22 μm nylon filter), and acidified with 50 µL of concentrated HCl. The magnetite solids were dissolved in 5 mL of 5 M HCl. In experiments with sorbed As(V), the magnetite was first equilibrated with the MOPS solution overnight, then As(V) was added and allowed to adsorb to the mineral for at least 5 hours, before the $^{57}Fe(II)$ was added to start the experiment.

After each experiment was completed, aqueous Fe and solid Fe were analyzed for Fe(II) and Fe(total) using the 1,10-phenanthroline method.[31, 32] The Fe isotope composition was analyzed using ICP-MS as described previously.[23, 24, 42, 43] To calculate the extent of Fe atom exchange, we applied the same approach as reported previously[24, 44] and described in short in the Electronic supplementary information (ESI). We are using only aqueous phase Fe isotope data to calculate the extent of Fe atom exchange because Fe(II) sorption to magnetite biases the solid phase isotope composition and results in an overestimation of the extent of Fe atom exchange.[15, 23, 45, 46] Particle sizes of magnetite were measured before and after Fe atom exchange reactions using transmission electron microscopy (TEM) and are reported in **Table S2**.

RESULTS AND DISCUSSION

Characterization of As(V) coprecipitated with and sorbed to magnetite. To evaluate how As binds to magnetite when it is coprecipitated compared to when it sorbs to magnetite, we used wet chemical extractions and As K-edge X-ray absorption spectroscopy (XAS). Here, we compare As-magnetite coprecipitates with pre-synthesized magnetite that was exposed to As(V)-containing solution at the same As:Fe mole ratio for 30 minutes.

We first confirmed that wet chemical extraction with NaOH selectively removes sorbed As as has been previously suggested.[29, 30] We extracted both As sorbed on magnetite, as well as As coprecipitated with magnetite (final As:Fe ratio of 0.0005, **Table S1**) with NaOH. We found that NaOH extracted 97±11% of the sorbed As compared to only 29±3% of the coprecipitated As (**Figure 1**). Complete dissolution of the magnetite recovered an additional 4±1% of the sorbed and 68±9% of the coprecipitated As, resulting in near complete As mass balance (99 and 100%, respectively). We obtained similar results using a higher As:Fe ratio (0.0099) where more than 90% of sorbed As(V) was extracted with NaOH and two thirds of the As remained in the coprecipitated magnetite (**Figure S2**). In both cases, total As recoveries were greater than 90% (**Table S3**). Note that our NaOH extraction resulted in almost double the amount of As incorporation previously derived from X-ray absorption spectra of coprecipitates with the same As:Fe ratio.[20] Our results indicate that extracting with NaOH recovers only sorbed As and can thus be used to distinguish between sorbed As and incorporated As. The results also suggest that up to 29% of the As in the coprecipitate were surface bound rather than incorporated.

To directly probe changes in As speciation before and after NaOH extraction, we collected As K-edge X-ray absorption (XAS) spectra for both coprecipitated and sorbed samples. For a qualitative evaluation, we compared the X-ray absorption near edge structure (XANES) (**Figure 2**; see **Figure S4** for the derivative spectra). The XANES spectra of the As-magnetite coprecipitate before and after extraction are highly similar, suggesting that the average As speciation remained the same after extraction (**Figure 2, middle panel**). The spectra show a shoulder at the rise of the edge, which is not observed in the adsorption sample and suggests that it may be due to incorporated As. The shoulder increased slightly after extraction (arrow d), suggesting a larger contribution of incorporated As(V) to the total spectrum and thus that the NaOH extraction removed predominantly the small fraction of sorbed As(V).

In contrast, the XANES spectra of sorbed As(V) before and after NaOH extraction differed significantly, particularly in the edge-rise region (arrow e in **Figure 2, lower panel**). Both wet chemical analysis (**Table S4**) and As fluorescence intensity (21 times smaller than before extraction, data not shown) suggest that only 2-5% of the initially added As(V) remained in the solid sample after NaOH extraction. Because of the low As content remaining, the EXAFS spectrum of the extracted solids has an insufficient signal-to-noise ratio for structural analysis (**Figure S3**). The marked decrease in As K_α fluorescence intensity and the observed differences in the XANES spectrum before and after extraction of the sorbed As provide further evidence to support NaOH extraction as an effective extractant for sorbed As(V).

We further compared the coprecipitated and sorbed As samples to several As reference materials including aqueous As(V) and the Fe-As(V) minerals scorodite and symplesite. The XANES spectra of the As magnetite samples and the As(V) references (**Figure 2, top panel**) all show an edge position (arrow a) and first major peak (white line, arrow b) at the same photon energy of 11,874 eV, indicative of As(V) being present in the samples. Sorbed As(V) and all As(V) reference materials exhibit similar spectral features in the pre-edge and absorption edge region (arrows a and b, respectively), indicating that As(V) was the predominant valence state in the samples and that As(V) reduction did not occur in reactions with pre-formed magnetite under the conditions of our study. Significant differences in the post-edge spectral region for sorbed As(V) and the As(V) standards, however, indicate the As(V) bonding in the sorbed samples is different than in aqueous As or the Fe-As minerals (arrows c in **Figure 2**). Because the hydration shells of a dissolved and an outer-sphere sorbed ion are the same and should therefore produce a similar spectrum, the significant spectral differences between magnetite-sorbed As(V) and the aqueous As(V) standard suggest that sorbed As(V) was bound as an inner-sphere complex. In addition, the sorbed As(V) spectrum is quite different from both the scorodite and symplesite spectra, suggesting that scorodite and symplesite do not precipitate in our sorption experiments. These results are further corroborated by the EXAFS data (discussed below).

Similar to the sorbed As samples, the XANES spectra indicate that As(V) bonding in the coprecipitated samples is different from aqueous As or the Fe-As mineral standards, as well as from sorbed As(V). The spectra of sorbed and coprecipitated As differ in both the pre-edge region (arrow d) and the post-edge region (arrows c). We can thus distinguish between sorbed and coprecipitated As and rule out the formation of distinct As-Fe phases during coprecipitation. The lack of As-Fe mineral phases in our samples is further supported by XRD patterns of the As(V)-magnetite coprecipitate, which are similar to that of magnetite precipitated in the absence of As(V) and show no reflections indicative of symplesite or scorodite formation (**Figure S1**).

Interestingly, the As(V)-magnetite coprecipitate samples exhibited a distinct shoulder in the pre-edge region of the XANES data (arrow d in **Figure 2,** dashed line in **Figure S4**). The position of the shoulder coincides with the white line of the As(III) standard As_2O_3, suggesting that partial reduction of As(V) to As(III) may have occurred (~20% As(III)/total As when interpreted by linear combination fitting, **Figure S5**). A similar shoulder in the XANES data equivalent to ~12-18% As(III) was previously observed in As(V)-magnetite samples coprecipitated by the same method and was assigned to beam-induced reduction due to the presence of cellulose used to dilute the sample.[20] For our measurements, however, we did not add organic material to the sample and we did not observe beam-induced evolution in our spectra. We also did not observe As(III) in the identically-mounted sorption samples, suggesting that beam-induced As(V) reduction is not the cause for the pre-edge shoulder. How As(V) might be reduced during coprecipitation from Fe(II)-Fe(III) solution is an intriguing question, particularly because neither aqueous Fe(II) nor magnetite or green rust are capable of As(V) reduction.[47-51] However, we only observed this feature in samples that were exposed to basic conditions (either during co-precipitation or following NaOH extraction), suggesting that As(V) reduction by Fe(II) may only be favorable under high pH

conditions and/or that a transient yet highly reactive Fe(II) phase such as $Fe(OH)_2$ may have formed and reduced a portion of As(V) to As(III).

While reduction of As(V) to As(III) is one possible explanation for the XANES pre-edge feature (arrow a in **Figure 2**), such features arise in the XANES of many elements for various structural reasons (review[52] and references therein). It is therefore possible that the XANES feature in the co-precipitated sample could arise due to a significantly different atomic coordination resulting from the incorporation of As(V) into a mineral. A combination of the two processes, i.e. reduction of As(V) to As(III) coupled with As(III) incorporation into magnetite, is unlikely as As(III) did not incorporate into biogenic magnetite that was formed from ferrihydrite[21] or during coprecipitation.[53] Based on the lack of previous evidence for either As(III) incorporation into magnetite or As(V) reduction by Fe(II) containing minerals, we suspect that the pre-edge shoulder in the XANES spectrum of As(V)-magnetite coprecipitates is more likely to be due to As(V) incorporation into the magnetite structure rather than As(V) reduction. Future work involving measurements of a broader standards dataset and *ab initio* modeling of both the XANES features and the energetics of the system may be able to provide further evidence for the consistency of the pre-edge shoulder with As(V) incorporation, but based on our current data and analysis we cannot make a definitive conclusion regarding the origin of the pre-edge XANES feature.

To further characterize the bonding environment of sorbed and coprecipitated As(V), we compared the Fourier transform (FT) of the EXAFS data to standards (**Figure 3**). All data show marked similarities in the structural features arising from the As(V) tetrahedron (main peak at R+dR = 1.25 Å, marked as 'O' in **Figure 3**), suggesting that AsO_4 is a rigid unit that has the same structure and disorder regardless of whether it is in solution, sorbed at a surface, or incorporated in a mineral. In addition to the main 'O' peak at R+dR = 1.25 Å (As-O distance R = 1.68 Å), the spectra show similar structure in the region R+dR = 1.6 – 2.5 Å, which is mostly due to multiple scattering (MS) within the As tetrahedron.[20] However, the spectra differ significantly in their second coordination or 'Fe shell' (**Figure 3**) at R+dR = 2.5-3.0 Å, which provides information on how the As(V) tetrahedron is bound to the Fe mineral. Our As(V) standards delimit the range of bonding environments expected in our samples, from no interaction with magnetite (aqueous As(V)) to fully incorporated via coordination to 4 or 5 Fe atoms at a distance of 3.31-3.39 Å in a bond through a shared tetrahedral O atom (scorodite[54] and symplesite[55]). While the aqueous As(V) standard shows little spectral contribution near R+dR = 2.8 Å, adsorbed and coprecipitated As(V) exhibit a significant peak in this region, which suggests inner-sphere complexation of As(V) in these samples. Spectra of both sorbed and coprecipitated As(V) in this spectral area rather show peaks similar to those in the scorodite and symplesite standards, which indicate the presence of As-Fe coordination and suggest inner-sphere complexation of As(V) to mineral Fe-O sites. The average As-Fe distance in the adsorbed and coprecipitated sample however appears larger than that in the scorodite standard (**Figure 3, arrow**).

The qualitative observations above were quantified in shell-by-shell fits of the EXAFS data using a two-shell model (O and Fe) that includes multiple-scattering contributions within the As(V) tetrahedron. The structural results from the fits are shown in Table 1 and the fit quality is illustrated in **Figure S6**. We can use the As-Fe distances determined in our samples to infer

the mechanism of As(V) association with the solids. For example, As(V) sorbed to an Fe oxide surface in a ^{2}C complex and As(V) in the scorodite structure both result in As-Fe distances of R = 3.36-3.38 Å.[56] The derived As-Fe distance for magnetite-sorbed As(V) of 3.38 Å (**Table 1**) is consistent with binding in the proposed ^{2}C complex[56], whereas the peak for the coprecipitate sample corresponds to a significantly longer As-Fe distance of 3.44 Å (**Table 1**). The longer As-Fe binding distance in our coprecipitate samples is closer to the Fe-Fe distance between tetrahedral and octahedral Fe in magnetite (3.47-3.49 Å[57]) and thus consistent with As substituted in the tetrahedral sites of magnetite in the coprecipitates. This interpretation is in agreement with previous analyses of XAS observations of magnetite-As coprecipitates synthesized by the same method.[20] Additionally, the distance mismatch between the tetrahedral Fe-O bonds in magnetite (1.88 Å) and the As-O bonds (1.68 Å) in an AsO_4 incorporation scenario can be compensated by local distortions in the Fe octahedra (**Figure S7**). The combined EXAFS evidence supports the NaOH extraction results indicating that the majority of As became incorporated during coprecipitation with magnetite, whereas As remained at the magnetite surface in our sorption experiments.

Redistribution of As in magnetite over time. Of interest beyond the initial incorporation of As(V) into mineral structures during their formation is the long term stability of As incorporated in magnetite. To determine whether incorporated As(V) redistributed from the magnetite structure to a sorbed, extractable phase on the magnetite surface over time, we used NaOH extractions as well as XAS to directly probe changes in As binding over time.

NaOH extractions revealed little change in the sorbed and incorporated As amounts over time in the coprecipitated magnetite samples, suggesting that arsenic was not redistributing between the magnetite surface and bulk structure (**Figure 4A and Table S3).** A small, but measurable increase in residual, or incorporated As(V) was observed for As(V) initially sorbed on magnetite. Over about 4 months, the amount of As in the magnetite structure increased from 3±0% to 13±1% (**Figure 4B and Table S3**). The observed increase in incorporated As(V) was accompanied by a decrease in sorbed As(V), suggesting that some of the sorbed As(V) became incorporated As over time. The overall As recovery in these experiments was about 90% (**Table S3**).

To directly measure whether structural changes in the As binding environment occurred over time, we collected XAS data on magnetite-sorbed As(V) reacted between 2 days and one month. The FT of the EXAFS data show an increase in both the amplitude of the Fe-shell peak (**Figure 5**) and the As-Fe distance with increasing reaction time (**Figure S8**). Structural modeling of the EXAFS data further suggests that longer reaction times result in an increase in Fe coordination number, which approaches the coordination number determined in the coprecipitate sample (**Table 1, Figure 6B**). The observed gradual change indicates a transition from an As coordination environment consistent with inner-sphere adsorption of As(V) at a reaction time of 30 minutes to a coordination environment increasingly similar to As(V) substituted into the magnetite structure after 3.5 to 28 days of reaction. The As-Fe distance also increased with reaction time, reached the largest value in the coprecipitation sample, and approached the Fe-Fe distance between tetrahedral and

octahedral Fe in magnetite (**Figure 6A**). The observed trends suggests that, over time, As(V) is being incorporated into the magnetite structure and into a similar binding environment as in the As-magnetite coprecipitate.

To estimate the extent of redistribution from sorbed to incorporated As species over time we performed linear combination (LC) fits of the EXAFS data from the 3.5 d and 28 d samples using the 30 minutes sorption and the coprecipitation samples as endmembers. The analysis showed that a relatively small contribution of the coprecipitation sample spectrum was needed to fit the spectrum, namely 5% and 8% in the 3.5 d and 28 d magnetite samples spectra, respectively (**Figure S9**). This fraction of the coprecipitate spectrum accounts for the observed increase over time in the signal from the Fe shell (**Figure S8)**. Given that a significant Fe signal is already present in the 30 minute sorption endmember, it is possible that the transformation from sorbed/labile to incorporated/stable As(V) species occurs with minimal change in the near-neighbor atomic coordination to which EXAFS is sensitive.

How sorbed As became increasingly incorporated into magnetite over time is an intriguing question. One possible mechanism is solid-state diffusion of As(V) into the magnetite structure, in analogy to diffusion of Fe(II) in magnetite, which has been hypothesized to contribute to the dynamic exchange between aqueous and solid phase Fe atoms in magnetite.[23] An alternative explanation is that Fe(II)-catalyzed recrystallization of magnetite or magnetite dissolution-reprecipitation enabled As incorporation, similar to previously reported incorporation of trace elements during recrystallization of goethite and hematite.[16, 17] To explore the role of aqueous Fe(II) for As redistribution over time, we conducted time-dependent experiments with sorbed and coprecipitated As(V) in the presence of 0.8-1.3 mM aqueous Fe(II) (range of final concentrations) and compared to our Fe(II)-free observations. Note that even in the Fe(II)-free reactors, we measured final aqueous Fe(II) concentrations of 0.1-0.2 mM, suggesting that a small portion of structural Fe(II) was released from the magnetite.

Similar to the Fe(II)-free reactors, we observed no measurable redistribution of As in the coprecipitate samples exposed to Fe(II) over the time frame of about four months (**Figure 4A, Table S3**). Initially sorbed As(V) was, however, again redistributed and became increasingly incorporated during the experiments with added aqueous Fe(II), reaching, within experimental error, similar intermediate and final extents of As incorporation as in the Fe(II)-free experiments (15% vs 13%, respectively after four months, **Figure 4B**). The striking similarities of our findings for As redistribution in the absence and presence of added aqueous Fe(II) suggest that aqueous Fe(II) had, overall, a minor effect on As redistribution for both coprecipitated and sorbed As(V).

The complete absence of As redistribution in the coprecipitate samples is in contrast to the reported release of incorporated metal ions, such as Co, Zn, Ni, Mn, and Cu from magnetite, goethite, and hematite in the presence of Fe(II).[14, 15, 23] The observed metal release was suggested to be related to the simultaneously occurring Fe(II)-catalyzed recrystallization of the Fe oxides and we thus monitored Fe atom exchange between magnetite and aqueous Fe(II) during our incorporation experiments using the enriched tracer approach.[23, 46] We observed only limited Fe atom exchange for As-coprecipitated magnetite (10-17 %, **Table S5**), which is consistent with extents of Fe atom exchange reported previously (9 %, data in

Table 2 of Gorski *et al*.[23] was re-evaluated with equations in Handler *et al*.[24]) and supports the finding of negligible As redistribution. Our observation of similarly limited Fe atom exchange for As-free and As-coprecipitated magnetite also suggests that the small extent of Fe atom exchange in As-magnetite coprecipitates was not caused by structurally incorporated As. In addition, release of Co from Co-containing magnetite under nominally identical experimental conditions as applied in our study only amounted to 10%, which would fall within the uncertainty of the As measurements (**Table S3, Figure 4A**) and would thus be non-detectable.

Similarly, we explored whether Fe(II)-catalyzed recrystallization of magnetite could play a role for the redistribution from sorbed to incorporated As. However, the low extents of Fe atom exchange of 10-11% during our redistribution experiments, both in the absence and presence of sorbed As(V) (**Table S5**), indicate that only a few outer atom layers of magnetite undergo Fe(II)-induced recrystallization. We therefore suggest that Fe(II)-catalyzed recrystallization of magnetite contributed only to a small extent to the observed redistribution of sorbed As(V).

The EXAFS data of sorbed As(V) in the presence of aqueous Fe(II) indicate no significant differences in the As(V) binding environment relative to the Fe(II)-free samples (**Figure S10**), in agreement with the negligible differences in As speciation as determined by NaOH extraction. Analysis of the EXAFS data showed that the As-Fe distance was almost identical in samples with and without added Fe(II) (**Figure 6A**). Similarly, the number of Fe coordination partners remains at a low value indicative of sorbed As(V) in the presence of aqueous Fe(II) over 7 days (**Figure 6B**). The combined spectroscopic evidence suggests that added Fe(II) had a negligible effect on the redistribution of As(V) in magnetite.

Because the reactors used for XAS analysis contained higher magnetite and aqueous As concentrations, with the latter at or above magnetite surface saturation (**Figure S11**), we subjected samples prepared under experimental conditions identical to XAS experiments to NaOH extraction. In agreement with negligible As incorporation detected by EXAFS, the extraction data also showed that only 2-3% of the added As became incorporated in the presence of aqueous Fe(II) (**Table S4**). At these high surface loadings (**Figure S11**), we observed a slight decrease in the extent of Fe atom exchange from 10-11% in the absence of As(V) to 4% (**Table S5**), suggesting that very high aqueous As(V) concentrations might negatively impact Fe atom exchange and redistribution of sorbed to incorporated As. Although the wet chemical and XAS data agree on the limited incorporation of initially sorbed As(V) in the presence of aqueous Fe(II), they do not provide a conclusive explanation for the increased and temporal increasing redistribution of sorbed to incorporated As in the absence of aqueous Fe(II).

Environmental Implications

We demonstrated that a high proportion of dissolved As(V) can become incorporated into the magnetite structure during coprecipitation. Once bound within the structure of magnetite, this As(V) was not be remobilized easily as sorbed or aqueous As in the presence of aqueous Fe(II), which is an abundant natural reductant. Our finding of limited As (re-)mobilization from As-magnetite coprecipitates is presumably due to the limited extent of

magnetite recrystallization. These findings have significant implications for As mobility in natural systems and during human-induced redox cycling of groundwater such as aquifer storage and recovery,[58, 59] where natural or induced redox cycling may yield significant quantities of mixed-valent Fe oxides. Furthermore, some iron oxide-based point-of-use As removal systems sequester and stabilize As predominantly in magnetite phases,[10] and the demonstrated absence of As mobilization from magnetite coprecipitates provides a potential mechanism in support of previous reports that the spent, As-enriched filter material can be safely disposed[8], which has been a matter of debate.[60]

While our wet chemical extraction data provides compelling evidence for tightly bound As in the magnetite structure, our XANES data is inconclusive as to whether only As(V) was incorporated during its coprecipitation with magnetite or whether As(III) may have been formed during this process. If the XANES pre-edge feature arises mainly due to a structural effect from incorporated As(V), current interpretations of XANES spectra of field or laboratory samples proposing the detection of mineral-bound As(III) might require reassessment. For example, the XANES-based identification of As(III) in As removal units[61] could be a misinterpretation of structural effects caused by magnetite-incorporated As(V) rather than evidence for As(V) reduction during coprecipitation from Fe(II)- and Fe(III)-containing solution and/or the incorporation of incompletely oxidized aqueous As(III). We therefore propose that coprecipitates of As(V) (or other elements) with the target minerals should be included as reference materials for XAS analysis and/or complementary techniques should be used to confirm the element's valence state. If, however, structural As(III) was indeed formed and incorporated into magnetite or a similar solid phase preferentially stabilized As(III), complete oxidation of As(III) to As(V) is not, as commonly suggested, a prerequisite for efficient As removal from the aqueous phase.[62] Confirming the formation of As(III) could open a new path for designing effective engineered systems for the removal of the more mobile As(III) species.

In contrast to the significant incorporation of divalent metal cations into the structure of many Fe oxides,[16, 17] the extent of redistribution of sorbed As(V) to incorporated into the magnetite structure was limited. The final amount of incorporated As(V) via redistribution was much lower than the amount of As incorporated during coprecipitation (13-15% and 64-68%, respectively), indicating that coprecipitation sequesters As more effectively and efficiently than sorption followed by redistribution. Because we observed similar amounts of As(V) incorporation in both the absence and presence of aqueous Fe(II), as well as a low extent of Fe(II)-catalyzed recrystallization of magnetite, Fe(II)-catalyzed recrystallization is most likely not a major driver of As(V) sequestration (or redistribution) in the environment.

Conflicts of interest

There are no conflicts of interest to declare.

Acknowledgements

We thank Drew Latta, Bhoopesh Mishra, and the MRCAT beamline staff for assistance during data collection at the synchrotron. This research was supported in part by the Subsurface Science Scientific Focus Area (SFA) at Argonne National Laboratory funded by the Subsurface Biogeochemical Research Program, Office of the Biological and Environmental Research,

Office of Science, U.S. Department of Energy (DOE), under contract DE-AC02-06CH11357. MRCAT/EnviroCAT operations are supported by DOE and the MRCAT/EnviroCAT member institutions.

References

1. Brammer H, Ravenscroft P. Arsenic in groundwater: A threat to sustainable agriculture in South and South-East Asia. Environment International. 2009;35:647-54.
2. Panaullah GM, Alam T, Hossain MB, Loeppert RH, Lauren JG, Meisner CA, Ahmed ZU, Duxbury JM. Arsenic toxicity to rice (Oryza sativa L.) in Bangladesh. Plant Soil. 2009;317:31-9.
3. BGS, DPHE. Arsenic contamination of groundwater in Bangladesh Vol 2 : Final report. In: Kinniburgh DG, Smedley PL, editors. British Geological Survey Technical Report WC/00/19. Keyworth: British Geological Survey; 2001.
4. Rahman MM, Chowdhury UK, Mukherjee SC, Mondal BK, Paul K, Lodh D, Biswas BK, Chanda CR, Basu GK, Saha KC, Roy S, Das R, Palit SK, Quamruzzaman Q, Chakraborti D. Chronic Arsenic Toxicity in Bangladesh and West Bengal, India—A Review and Commentary. Journal of Toxicology: Clinical Toxicology. 2001 2001/01/01;39(7):683-700.
5. Smedley PL, Kinniburgh DG. A review of the source, behaviour and distribution of arsenic in natural waters. Appl Geochem. 2002;17:517-68.
6. van Genuchten CM, Peña J, Amrose SE, Gadgil AJ. Structure of Fe(III) precipitates generated by the electrolytic dissolution of Fe(0) in the presence of groundwater ions. Geochim Cosmochim Acta. 2014 2/15/;127:285-304.
7. Nikolaidis NP, Dobbs GM, Lackovic JA. Arsenic removal by zero-valent iron: field, laboratory and modeling studies. Wat Res. 2003;37(6):PII S0043-1354(02)00483-9. PubMed PMID: WOS:000181460700022.
8. Hussam A, Munir AKM. A simple and effective arsenic filter based on composite iron matrix: Development and deployment studies for groundwater of Bangladesh. Journal of Environmental Science and Health Part A. 2007;42:1869-78. PubMed PMID: WOS:000250556000019.
9. Sun J, Chillrud SN, Mailloux BJ, Stute M, Singh R, Dong H, Lepre CJ, Bostick BC. Enhanced and stabilized arsenic retention in microcosms through the microbial oxidation of ferrous iron by nitrate. Chemosphere. 2016 2//;144:1106-15.
10. Neumann A, Kaegi R, Voegelin A, Hussam A, Munir AKM, Hug SJ. Arsenic Removal with Composite Iron Matrix Filters in Bangladesh: A Field and Laboratory Study. Environ Sci Technol. 2013 2013/05/07;47(9):4544-54.
11. Rawson J, Prommer H, Siade A, Carr J, Berg M, Davis JA, Fendorf S. Numerical Modeling of Arsenic Mobility during Reductive Iron-Mineral Transformations. Environ Sci Technol. 2016 2016/03/01;50(5):2459-67.
12. Hansel CMCM, Benner SGSG, Fendorf S. Competing Fe(II)-Induced Mineralization Pathways of Ferrihydrite. Environ Sci Technol. 2005;39:7147-53.
13. Tamaura Y, Ito K, Katsura T. Transformation of γ-FeO(OH) to Fe_3O_4 by Adsorption of Iron(II) Ion on γ-FeO(OH). Chem Soc Dalton Trans. 1983:189-94.
14. Frierdich AJ, Catalano JG. Controls on Fe(II)-Activated Trace Element Release from Goethite and Hematite. Environ Sci Technol. 2011 2012/02/07;46(3):1519-26.
15. Latta DE, Gorski CA, Scherer MM. Influence of Fe^{2+}-catalyzed iron oxide recrystallization on metal cycling. Biochem Soc T. 2012;40:1191-7. PubMed PMID: 23176453.
16. Frierdich AJ, Luo Y, Catalano JG. Trace element cycling through iron oxide minerals during redox-driven dynamic recrystallization. Geology. 2011;39:1083-6. en.
17. Um W, Chang H-S, Icenhower JP, Lukens WW, Serne RJ, Qafoku NP, Westsik JH, Buck EC, Smith SC. Immobilization of 99-technetium(VII) by Fe(II)-goethite and limited reoxidation. Environ Sci Technol. 2011;45:4904-13. PubMed PMID: 21557602.
18. Catalano JG, Luo Y, Otemuyiwa BT. Effect of aqueous Fe(II) on arsenate sorption on goethite and hematite. Environ Sci Technol. 2011;45(20):8826-33.

19. Prucek R, Tuček J, Kolařík J, Filip J, Marušák Z, Sharma VK, Zbořil R. Ferrate(VI)-Induced Arsenite and Arsenate Removal by In Situ Structural Incorporation into Magnetic Iron(III) Oxide Nanoparticles. Environ Sci Technol. 2013;47:3283-92. PubMed PMID: 23451768.
20. Wang Y, Morin G, Ona-Nguema G, Juillot F, Calas G, Brown GE. Distinctive arsenic(V) trapping modes by magnetite nanoparticles induced by different sorption processes. Environ Sci Technol. 2011;45:7258-66. PubMed PMID: 21809819.
21. Coker VS, Gault AG, Pearce CI, Van der Laan G, Telling ND, Charnock JM, Polya DA, Lloyd JR. XAS and XMCD evidence for species-dependent partitioning of arsenic during microbial reduction of ferrihydrite to magnetite. Environ Sci Technol. 2006;40:7745-50.
22. Pedersen HD, Postma D, Jakobsen R. Release of arsenic associated with the reduction and transformation of iron oxides. Geochim Cosmochim Acta. 2006;70:4116-29.
23. Gorski CA, Handler RM, Beard BL, Pasakarnis T, Johnson CM, Scherer MM. Fe Atom Exchange between Aqueous Fe^{2+} and Magnetite. Environ Sci Technol. 2012;46:12399-407. PubMed PMID: 22577839.
24. Handler RM, Frierdich AJ, Johnson CM, Rosso KM, Beard BL, Wang C, Latta DE, Neumann A, Pasakarnis T, Premaratne WAPJ, Scherer MM. Fe(II)-Catalyzed Recrystallization of Goethite Revisited. Environ Sci Technol. 2014 Oct 7;48(19):11302-11. PubMed PMID: WOS:000343016600037.
25. Gorski CA, Scherer MM. Influence of Magnetite Stoichiometry on Fe-II Uptake and Nitrobenzene Reduction. Environ Sci Technol. 2009;43(10):3675-80. PubMed PMID: WOS:000266046700045.
26. Pichler T, Veizer JAN, Hall GEM. Natural Input of Arsenic into a Coral-Reef Ecosystem by Hydrothermal Fluids and Its Removal by Fe (III) Oxyhydroxides. 1999;33:1373-8.
27. Bowell R. Sorption of arsenic by iron oxides and oxyhydroxides in soils. Appl Geochem. 1994;9.
28. Gorski CA, Scherer MM. Determination of nanoparticulate magnetite stoichiometry by Mossbauer spectroscopy, acidic dissolution, and powder X-ray diffraction: A critical review. Am Mineral. 2010;95:1017-26.
29. Jackson BP, Miller WP. Effectiveness of Phosphate and Hydroxide for Desorption of Arsenic and Selenium Species from Iron Oxides. Soil Sci Soc Am J. 2000;64(5):1616-22. English.
30. Van Herreweghe S, Swennen R, Vandecasteele C, Cappuyns V. Solid phase speciation of arsenic by sequential extraction in standard reference materials and industrially contaminated soil samples. Environmental Pollution. 2003 4//;122(3):323-42.
31. Tamura H, Goto K, Yotsuyan.T, Nagayama M. Spectrophotometric Determination of Iron(II) with 1,10-Phenanthroline in Presence of Large Amounts of Iron(III). Talanta. 1974;21:314-8.
32. Schilt AA. Applications of 1,10-phenanthroline and related compounds. 1st ed. Oxford: Pergamon Press; 1969.
33. Brown RJC, Yardley RE, Brown AS, Milton MJT. Sample matrix and critical interference effects on the recovery and accuracy of concentration measurements of arsenic in ambient particulate samples using ICP-MS. Journal of Analytical Atomic Spectrometry. 2004;19:703.
34. Cai Y, Georgiadis M, Fourqurean JW. Determination of arsenic in seagrass using inductively coupled plasma mass spectrometry. Spectrochimica Acta Part B: Atomic Spectroscopy. 2000;55:1411-22.

35. Kandegedara A, Rorabacher DB. Noncomplexing tertiary amines as "better" buffers covering the range of pH 3-11. Temperature dependence of their acid dissociation constants. Anal Chem. 1999;71(15):3140-4. PubMed PMID: WOS:000081877100040.
36. Segre CU, Leyarovska NE, Chapman LD, Lavender WM, Plag PW, King AS, Kropf AJ, Bunker BA, Kemner KM, Dutta P, Duran RS, Kaduk J. The MRCAT insertion device beamline at the Advanced Photon Source. In: Pianetta P, editor. Synchrotron Radiation Instrumentation: Eleventh US National Conference; New York: American Institute of Physics; 2000. p. 419-22.
37. O'Loughlin EJ, Kelly SD, Cook RE, Csencsits R, Kemner KM. Reduction of Uranium(VI) by mixed iron(II/iron(III) hydroxide (green rust): Formation of UO2 nanoparticles. Environ Sci Technol. 2003;37(4):721-7.
38. Newville M, Livins P, Yacoby Y, Rehr JJ, Stern EA. Near-edge x-ray absorption fine structure of Pb – a comparison of theory and experiment. Phys Rev B. 1993;47(21):14126-31.
39. Kitahama K, Kiriyama R, Baba Y. Refinement of crystal-structure of scorodite. Acta Cryst B. 1975;31:322-4.
40. Ankudinov AL, Ravel B, Rehr JJ, Conradson SD. Real-space multiple-scattering calculation and interpretation of x-ray absorption near-edge structure. Phys Rev B. 1998;58(12):7565-76.
41. Newville M, Ravel B, Haskel D, Stern EA. Analysis of multiple scattering XAFS data using theoretical standards. Physica B. 1995;208/209:154-6.
42. Frierdich AJ, Helgeson M, Liu C, Wang C, Rosso KM, Scherer MM. Iron Atom Exchange between Hematite and Aqueous Fe(II). Environ Sci Technol. 2015 2015/07/21;49(14):8479-86.
43. Latta DE, Bachman JE, Scherer MM. Fe Electron Transfer and Atom Exchange in Goethite: Influence of Al-Substitution and Anion Sorption. 2012.
44. Mikutta C, Wiederhold JG, Cirpka OA, Hofstetter TB, Bourdon B, von Gunten U. Iron isotope fractionation and atom exchange during sorption of ferrous iron to mineral surfaces. Geochim Cosmochim Acta. 2009;73:1795-812.
45. Crosby HA, Johnson CM, Roden EE, Beard BL. Coupled Fe(II)-Fe(III) electron and atom exchange as a mechanism for Fe isotope fractionation during dissimilatory iron oxide reduction. Environ Sci Technol. 2005;39:6698-704.
46. Handler RM, Beard BL, Johnson CM, Scherer MM. Atom exchange between aqueous Fe(II) and goethite: An Fe isotope tracer study. Environ Sci Technol. 2009;43:1102-7.
47. Amstaetter K, Borch T, Larese-Casanova P, Kappler A. Redox Transformation of Arsenic by Fe(II)-Activated Goethite (a-FeOOH). Environ Sci Technol. 2010;44(1):102-8.
48. Wang Y, Morin G, Ona-Nguema G, Juillot F, Guyot F, Calas G, Brown GE. Evidence for Different Surface Speciation of Arsenite and Arsenate on Green Rust: An EXAFS and XANES Study. Environ Sci Technol. 2010 2010/01/01;44(1):109-15.
49. Liu C-H, Chuang Y-H, Chen T-Y, Tian Y, Li H, Wang M-K, Zhang W. Mechanism of Arsenic Adsorption on Magnetite Nanoparticles from Water: Thermodynamic and Spectroscopic Studies. Environ Sci Technol. 2015 2015/07/07;49(13):7726-34.
50. Su CM, Puls RW. Arsenate and arsenite sorption on magnetite: Relations to groundwater arsenic treatment using zerovalent iron and natural attenuation. Water Air Soil Pollut. 2008 Sep;193(1-4):65-78. PubMed PMID: ISI:000257961200007.
51. Kocar BD, Fendorf S. Thermodynamic Constraints on Reductive Reactions Influencing the Biogeochemistry of Arsenic in Soils and Sediments. Environ Sci Technol. 2009;43:4871-7.
52. Sarangi R. X-ray absorption near-edge spectroscopy in bioinorganic chemistry: Application to M–O2 systems. Coordination Chemistry Reviews. 2013 1/15/;257(2):459-72.

53. Wang YH, Morin G, Ona-Nguema G, Menguy N, Juillot F, Aubry E, Guyot F, Calas G, Brown GE. Arsenite sorption at the magnetite–water interface during aqueous precipitation of magnetite: EXAFS evidence for a new arsenite surface complex. Geochim Cosmochim Acta. 2008;72(11):2573-86.
54. Xu Y, Zhou G-P, Zheng X-F. Redetermination of iron(III) arsenate dihydrate. Acta Crystallographica Section E. 2007;63(3):i67-i9.
55. Mori H, Ito T. The structure of vivianite and symplesite. Acta Crystallographica. 1950;3(1):1-6.
56. Sherman DM, Randall SR. Surface complexation of arsenie(V) to iron(III) (hydr)oxides: Structural mechanism from ab initio molecular geometries and EXAFS spectroscopy. Geochim Cosmochim Acta. 2003;67(22):4223-30.
57. Haavik C, Stølen S, Fjellvåg H, Hanfland M, Häusermann D. Equation of state of magnetite and its high-pressure modification: Thermodynamics of the Fe-O system at high pressure. Am Mineral. 2000;85(3-4):514-23.
58. Arthur JD, Dabous AA, Cowart JB. Mobilization of arsenic and other trace elements during aquifer storage and recovery, southwest Florida. Sacramento, CA2002.
59. Wallis I, Prommer H, Pichler T, Post V, Norton SB, Annable MD, Simmons CT. Process-based reactive transport model to quantify arsenic mobility during aquifer storage and recovery of potable water. Environ Sci Technol. 2011;45:6924-31. PubMed PMID: 21718078.
60. Amrose S, Burt Z, Ray I. Safe Drinking Water for Low-Income Regions. In: Gadgil A, Tomich TP, editors. Annual Review of Environment and Resources, Vol 40. Annual Review of Environment and Resources. 40. Palo Alto: Annual Reviews; 2015. p. 203-31.
61. Neumann A, Olson TL, Scherer MM. Spectroscopic Evidence for Fe(II)–Fe(III) Electron Transfer at Clay Mineral Edge and Basal Sites. Environ Sci Technol. 2013 2013/07/02;47(13):6969-77.
62. Hug SJ, Leupin OX, Berg M. Bangladesh and Vietnam: Different groundwater compositions require different approaches to arsenic mitigation. Environ Sci Technol. 2008;42(17):6318-23. PubMed PMID: WOS:000258883300008.

Table 1. Structural modeling of the EXAFS data.

Shell	N	R(Å)	σ^2 (Å^2)	ΔE(eV)[c]	DF	R-factor
Aqueous As^V						
O	4.0 [a]	1.69 ± 0.01	0.0032 ± 0.0005	-0.4 ± 0.9	9	0.004
Scorodite						
O	4.0 [a]	1.69 ± 0.01	0.0022 ± 0.0002	0.5 ± 0.6	8	0.003
Fe	4.0 [a]	3.35 ± 0.02	0.0063 ± 0.001			
As^V + magnetite, adsorption, 30 min						
O	4.0 [a]	1.70 ± 0.01	0.0022 ± 0.0002	0.3 ± 0.7	8	0.003
Fe	1.2 ± 0.3	3.38 ± 0.01	0.0063[b]			
As^V + magnetite, adsorption, 3.5 days						
O	4.0 [a]	1.70 ± 0.01	0.0023 ± 0.0002	0.4 ± 0.5	8	0.002
Fe	1.7 ± 0.2	3.39 ± 0.01	0.0063[b]			
As^V + magnetite, adsorption, 4 weeks						
O	4.0 [a]	1.70 ± 0.01	0.0023 ± 0.0002	0.6 ± 0.8	8	0.004
Fe	2.0 ± 0.3	3.40 ± 0.01	0.0063[b]			
As^V + magnetite, coprecipitation						
O	4.0 [a]	1.70 ± 0.01	0.0032 ± 0.0004	-0.4 ± 0.8	8	0.007
Fe	3.1 ± 0.4	3.43 ± 0.01	0.0063[b]			

N, R, and σ^2 are coordination number, radial distance, and Debye-Waller factor, respectively, for each path used in the fit. ΔE is the energy shift relative to the calculated Fermi level. DF = degrees of freedom in the fit, i.e. the difference between the number of independent data points and the number of fit parameters. The R-factor is the fractional misfit of the data relative to its amplitude, a goodness-of-fit indicator. More details on these fit parameters can be found in FEFFIT's documentation.[41]

[a] Held fixed to the O coordination number in the As^V tetrahedron or to the As-Fe coordination number in scorodite.

[b] Held fixed to the value shown, which is the value obtained when the scorodite standard is fit without constraints on the Debye-Waller factor.

[c] The ΔE for the O and Fe paths were both refined but constrained to be equal.

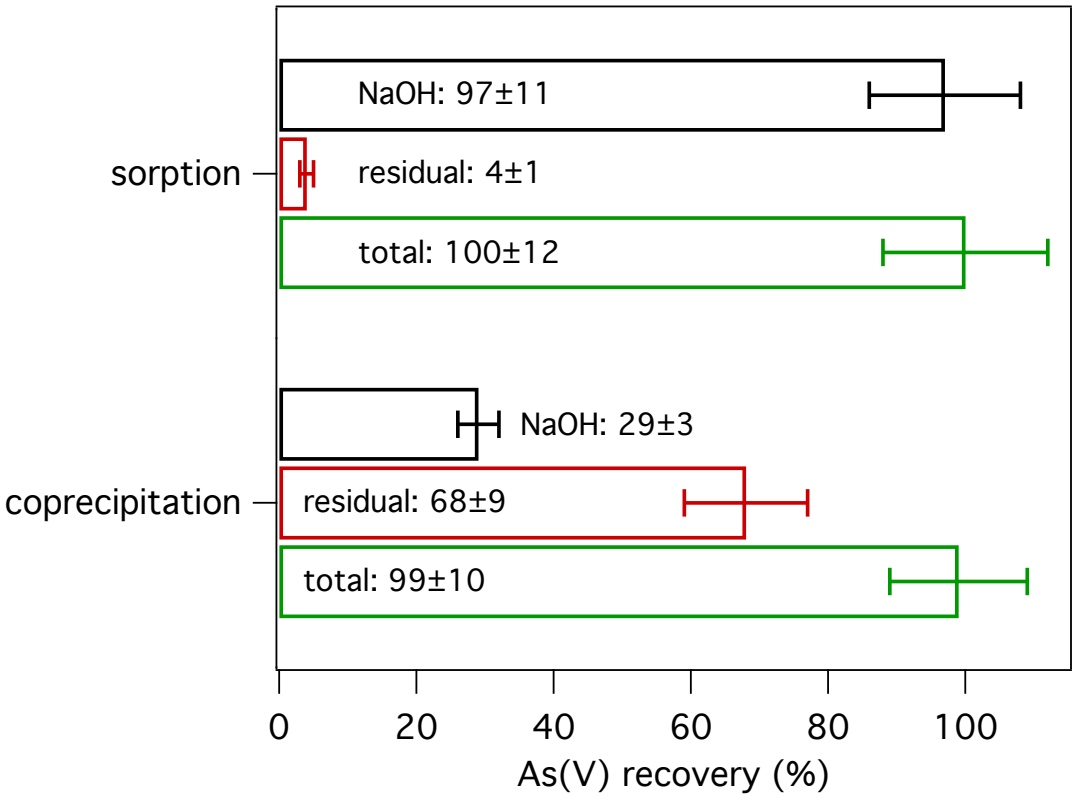

Figure 1. As recovered from magnetite with sorbed As(V) (30 minutes) and As(V)-magnetite coprecipitates in the NaOH extraction step and subsequent total dissolution. In both experiments, the molar As:Fe ratio was 0.0005 and the overall total As recovery was ≥99%. (Similar results were obtained for a molar As:Fe ratio of 0.099, see **Figure S2**)

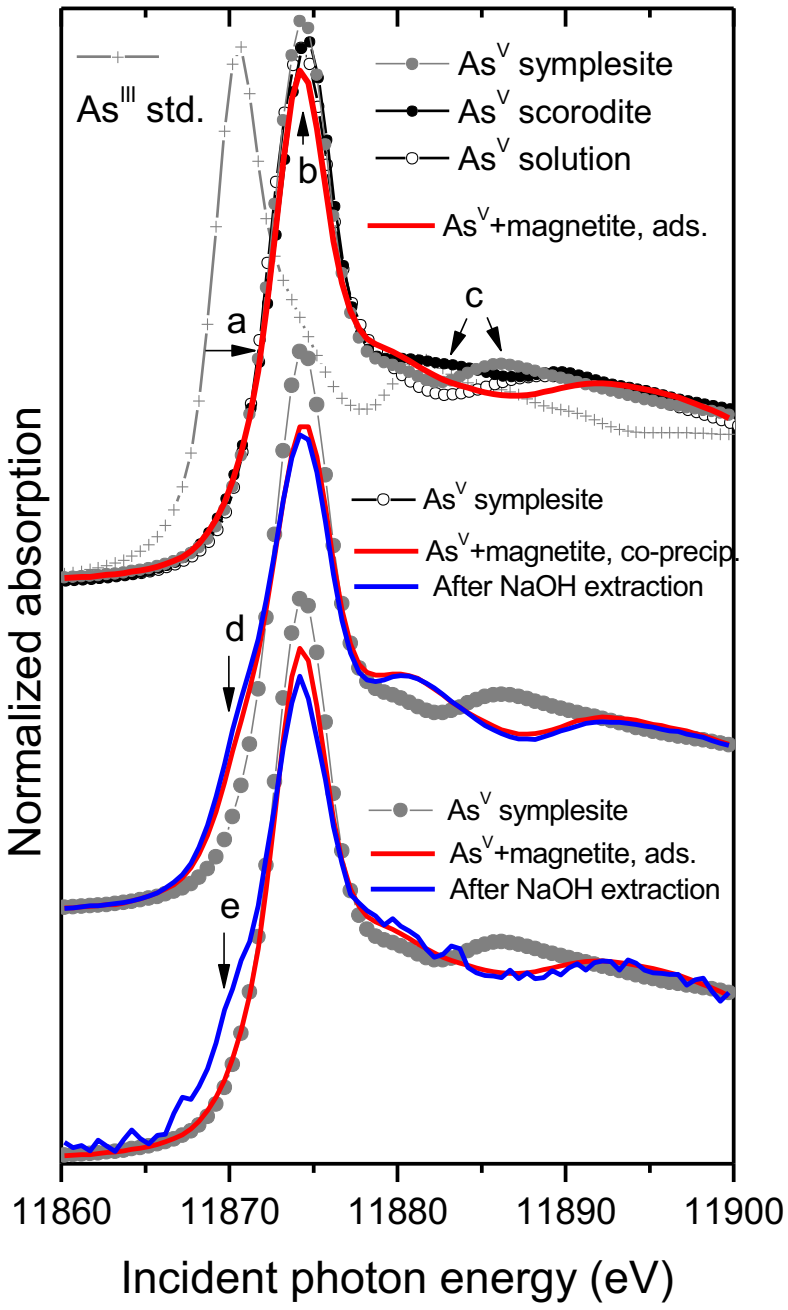

Figure 2. Comparisons of the As K-edge XANES spectra from the adsorption and co-precipitation magnetite reactors (lines) to As(III) and As(V) standards (symbols). Magnetite with sorbed As(V) and As(V)-magnetite coprecipitate (As:Fe mole ratio of 0.007) samples are shown before and after extraction with NaOH. The arrows indicate spectral features that are discussed in the text.

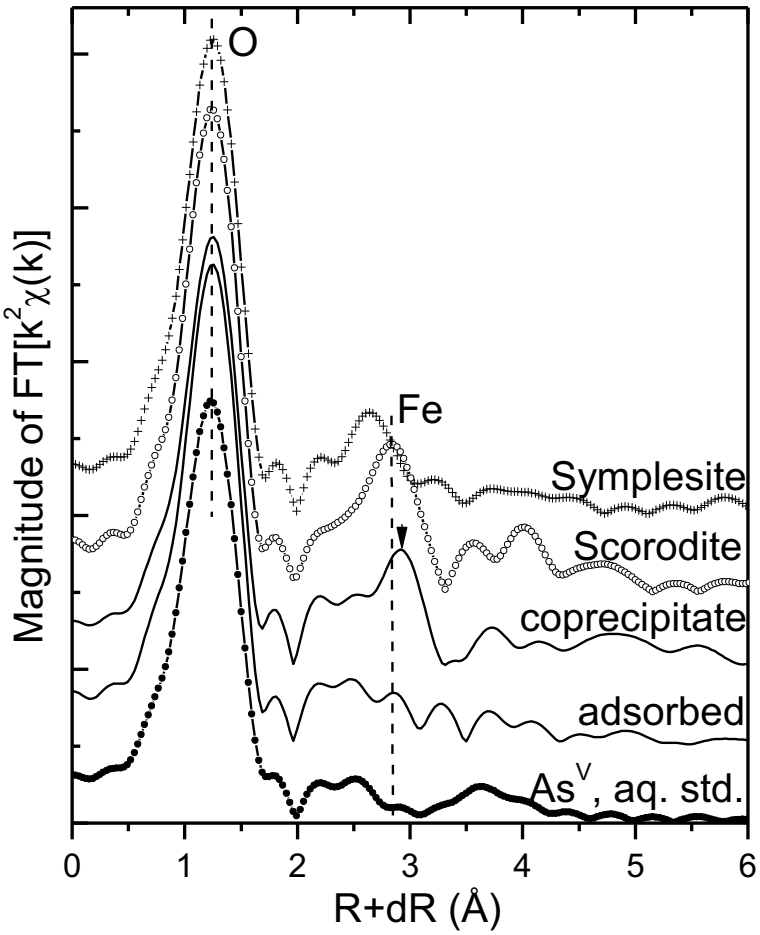

Figure 3. Fourier transform of the k^2-weighed As K-edge EXAFS data of sorbed As(V) and magnetite coprecipitated As(V) as well as As reference materials (aqueous As(V), Fe-As phases symplesite and scorodite). The vertical dashed lines indicate the peaks corresponding to the O and Fe coordination shells in scorodite. Experimental data presented as solid lines and standards as lines with symbols. (For real part of FT data, see **Figure S8**.

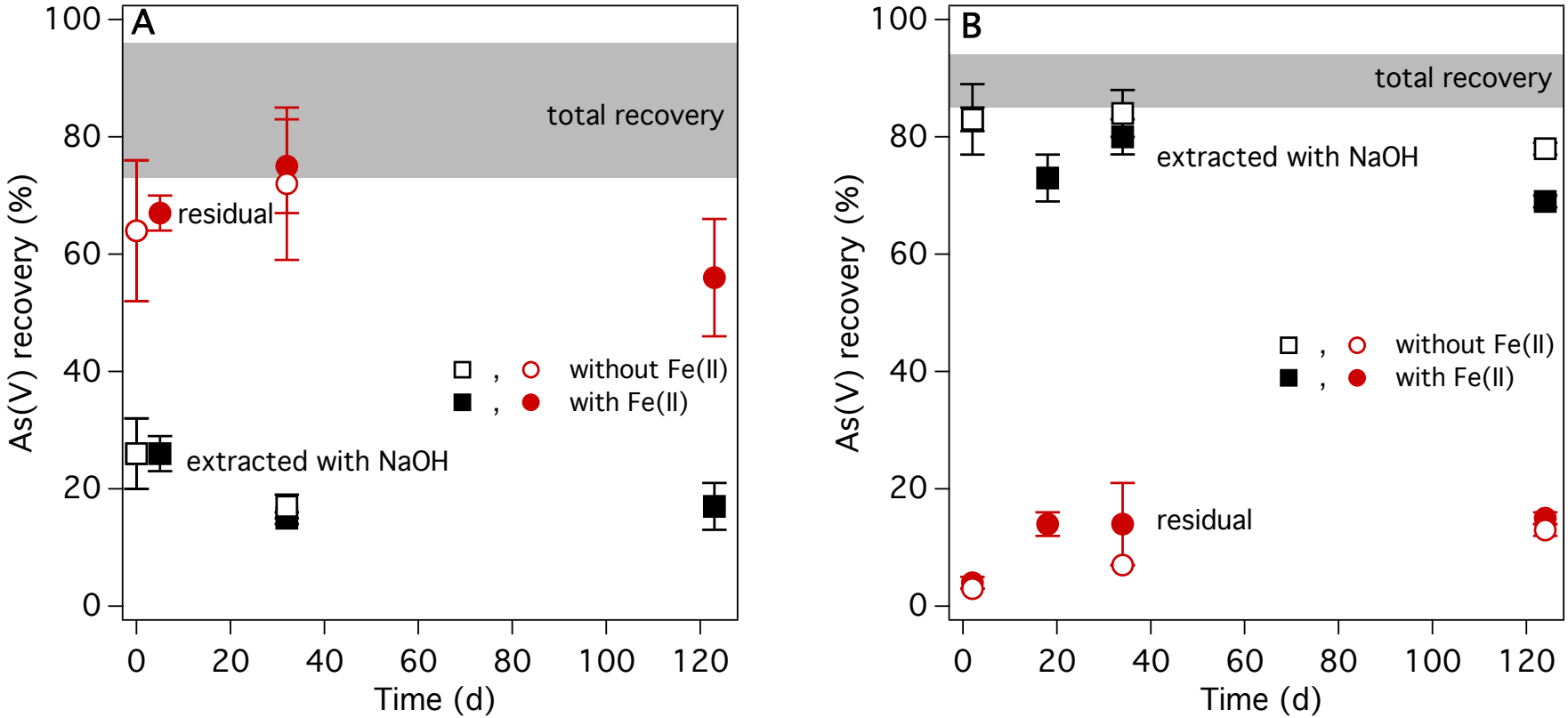

Figure 4. As(V) redistribution in magnetite in the absence (open markers) and presence (solid markers) of aqueous Fe(II). A: As(V) coprecipitated with magnetite (As:Fe mole ration of 0.0099) remains incorporated in magnetite over the time frame of the experiment, both in the presence and absence of aqueous Fe(II). B: Up to 15% of aqueous and magnetite-sorbed As(V) (initial concentration of 13.3 μM) become incorporated into the magnetite structure over 124 days of experiment, both in the presence and absence of aqueous Fe(II). Reaction conditions: 1 g/L magnetite, pH 7.2

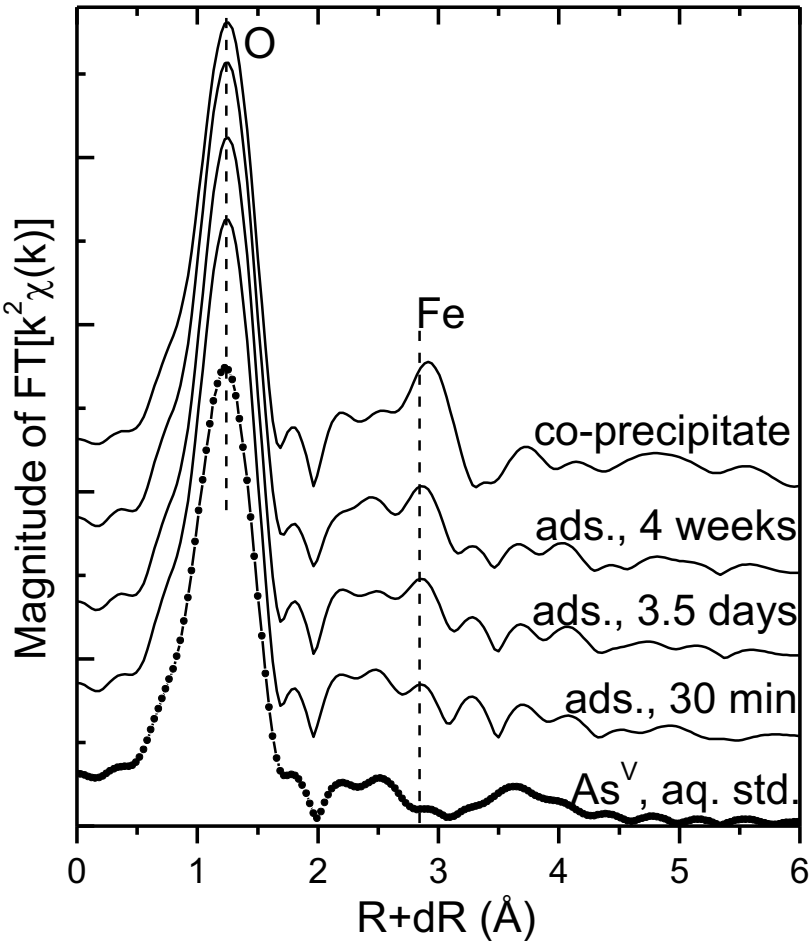

Figure 5. Fourier transform of the k^2-weighed As K-edge EXAFS data of As(V) adsorbed to magnetite. The vertical dashed lines indicate the peaks corresponding to the O and Fe coordination shells. The data show an evolution from an As coordination environment consistent with inner-sphere adsorption of As(V) at a reaction time of 30 minutes to a coordination environment increasingly similar to As(V) substituted into the magnetite structure after 3.5 days and 4 weeks of reaction. (For real part of FT data, see **Figure S8**.)

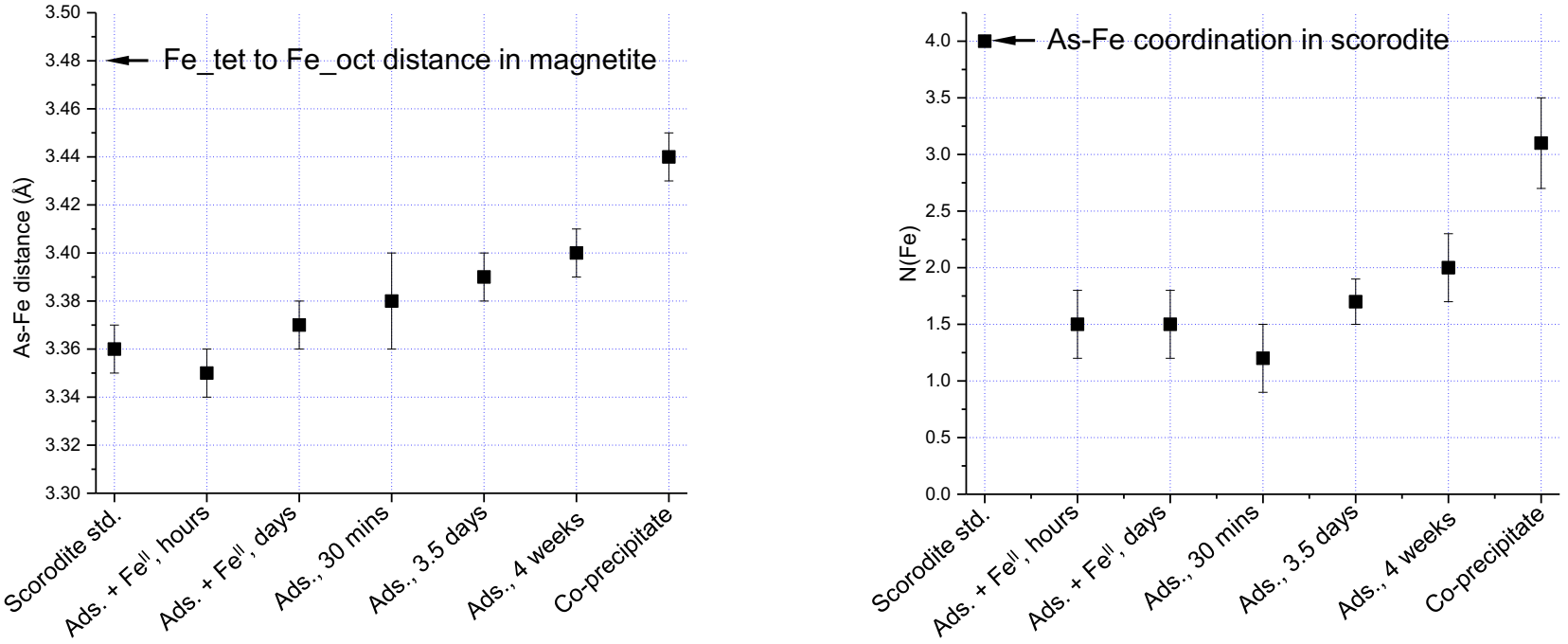

Figure 6. Structural modeling of the EXAFS data from sorbed As(V) in the absence and presence of aqueous Fe(II) and As(V)-magnetite coprecipitate. A: Refined As-Fe distances, which are compared to the As-Fe distance in scorodite and the Fe-Fe distance between tetrahedral and octahedral Fe in magnetite[57]. B: As-Fe coordination numbers resulting from the shell-by-shell fit of the data.

Electronic supplementary information

As(V) in Magnetite: Incorporation and Redistribution

Brittany L. Huhmann[1,2#], Anke Neumann[3#], Maxim I. Boyanov[4,5], Kenneth M. Kemner[4], and Michelle M. Scherer[1]*

[1]Department of Civil and Environmental Engineering, University of Iowa, Iowa City, IA, 52242, United States

[2]*Present Address:* Department of Civil and Environmental Engineering, Massachusetts Institute of Technology, Cambridge, MA, 02139, United States

[3]School of Engineering, Newcastle University, Newcastle upon Tyne, NE1 7RU, United Kingdom

[4]Biosciences Division, Argonne National Laboratory, Argonne, IL, 60439, United States

[5]*Institute of Chemical Engineering, Bulgarian Academy of Sciences, Sofia 1113, Bulgaria*

[#]*Author Contributions*: Brittany Huhmann and Anke Neumann contributed equally to this work.

[*]*Corresponding Author*: phone: +44 191 208 6406; email: anke.neumann@ncl.ac.uk

This document contains:
Text on the Calculation of the extent of Fe atom exchange
5 Tables
11 Figures

Methods

Calculation of the extent of Fe atom exchange

The Fe isotope composition was analyzed on the ICP-MS as described previously[1-4] and is reported as Fe isotope fraction for isotope *i*:

$$f^i\mathrm{Fe} = \frac{^i\mathrm{counts}}{^{54}\mathrm{counts} + ^{56}\mathrm{counts} + ^{57}\mathrm{counts} + ^{58}\mathrm{counts}} \quad \text{(eq 1)}$$

To quantify the extent of Fe atom exchange between magnetite and aqueous Fe(II), we used the mass balance approach as previously described:[3,5]

$$Percent\ Magnetite\ Fe\ Exchange = \frac{N_{Fe(II)_{aq}} \times (f^iFe(II)^{ini}_{aq} - f^iFe(II)^{t}_{aq})}{N^{tot}_{Mag} \times (f^iFe(II)^{t}_{aq} - f^iFe^{ini}_{Mag})} \times 100 \quad \text{(eq 2)}$$

Here, $f^iFe(II)^{ini}_{aq}$, $f^iFe(II)^{t}_{aq}$, and $f^iFe^{ini}_{Mag}$ are the initial fraction of isotope *i* in aqueous Fe(II), the fraction of isotope *i* in aqueous Fe(II) at time t, and the initial fraction of isotope *i* in magnetite, respectively. $N_{Fe(II)_{aq}}$ and N^{tot}_{Mag} are the moles of Fe(II) added to solution and the moles of Fe in magnetite in the system. The "system" refers to the components that have participated in exchange and are at equilibrium after mixing.[3]

Table S1. Properties of magnetite used in this study (± 1 standard deviation, when given).

	Synthesis Parameters				Solid properties			
Sample ID	As:Fe mole ratio	pH	Temp. (°C)	Aging Time (day)	As:Fe mole ratio[a]	BET Surface area (m^2/g)	Stoichiometry (x[b])	Identity Confirmed by XRD?
Magnetite	0	10-11	Room temp.	1	n.m.[c]	65.30	0.45 ± 0.02[d]	Y
As(V)-Magnetite Coprecipitate	0.0011	10-11	Room temp.	1	0.0005 ± 0.00001[e]	n.m.	0.49 ± 0.04[d]	N
As(V)-Magnetite Coprecipitate	0.0070	10-11	Room temp.	1	n.m.	n.m.	n.m.	Y
As(V)-Magnetite Coprecipitate	0.0100	10-11	Room temp.	1	0.0099 ± 0.00153[d]	n.m.	0.50 ± 0.03[d]	Y

[a] As:Fe mole ratio determined by dissolution in HCl. As(V) concentration was measured on ICP-MS and Fe concentration was measured spectrophotometrically by the phenanthroline method.

[b] Magnetite Fe(II) content as defined by $x = \frac{{}^{Oct}Fe(II)}{{}^{Oct}Fe(III)+{}^{Tet}Fe(III)}$

[c] Not measured.

[d] Mean and one standard deviation of triplicate reactors of 15 mg magnetite dissolved in 5 M HCl.

[e] Mean and one standard deviation of triplicate reactors of 10 mg magnetite dissolved in 5 M HCl.

Table S2. Particle sizes.

	Diameter (nm)
Magnetite	11.3 (3.6)
Magnetite + 100 µM adsorbed As(V) + Fe(II), 7 d	9.3 (3)
As(V)-Magnetite Coprecipitate (0.0099)	8.7 (2.4)

Table S3. NaOH extractions of As(V) from magnetite following adsorption and coprecipitation, in the presence and absence of aqueous Fe(II).

		Initial added	Final Aqueous		NaOH extraction *"adsorbed"*		Residual solids *"incorporated"*		Total recovery	
		nmol	nmol	%	nmol	%	nmol	%	nmol	%
As(V) Coprecipitates										
As:Fe mole ratio = 0.0005	Adsorption Control	98	0(0)	0(0)	95(11)	97(11)	3(1)	4(1)	98(12)	100(12)
	Coprecipitate	64	---	---	18(2)	29(3)	44(5)	68(9)	64(7)	99(12)
As:Fe mole ratio = 0.0099	Adsorption Control	1912	31(28)	2(1)	1778(39)	93(1)	100(2)	5(0)	1909(12)	100(1)
	Coprecipitate	2055	---	---	524(116)	26(6)	1318(253)	64(12)	1842(368)	90(18)
	t = 32 d	2055	1(0)	0(0)	344(44)	17(2)	1472(260)	72(13)	1816 (303)	88(15)
	Coprecipitate + Fe(II)									
	t = 5 d	2055	0(0)	0(0)	538(63)	26(3)	1375(67)	67(3)	1914(88)	96(5)
	t = 32 d	2055	0(0)	0(0)	308(30)	15(1)	1540(150)	75(8)	1847(189)	90(9)
	t = 123 d	2055	0(0)	0(0)	352(75)	17(4)	1155(214)	56(10)	1507(279)	73(14)
Adsorbed As(V)										
As(V) concentration = 13.3 µM	Adsorbed As(V)									
	t = 2 d	200	8(15)	4(7)	165(12)	83(6)	5(1)	3(0)	182(2)	91(1)
	t = 34 d	200	0(0)	0(0)	168(8)	84(4)	13(1)	7(0)	182(8)	91(4)
	t = 124 d	200	0(0)	0(0)	156(3)	78(1)	25(1)	13(1)	182(3)	91(1)
	Adsorbed As(V) + Fe(II)									
	t = 2 d	200	0(0)	0(0)	165(5)	83(2)	7(1)	4(1)	179(4)	89(2)
	t = 18 d	200	0(0)	0(0)	146(7)	73(4)	27(4)	14(2)	173(11)	87(6)
	t = 34 d	200	0(0)	0(0)	160(6)	80(3)	28(15)	14(7)	187(20)	94(10)
	t = 124 d	200	0(0)	0(0)	139(3)	69(1)	31(1)	15(1)	170(3)	85(2)

Table S4. NaOH extractions of As(V) from magnetite following adsorption under experimental conditions identical to sample preparation for XAS analysis. Experimental conditions: 10 g L^{-1} magnetite, 1 mM Fe(II), in 15 mL 50 mM MOPS at pH 7.2

		Initial added	Final Aqueous		NaOH extraction *"adsorbed"*		Residual solids *"incorporated"*		Total recovery	
		nmol	nmol	%	nmol	%	nmol	%	nmol	%
	Adsorbed As(V) + Fe(II)									
As(V) concentration = 2933 μM	t = 0 d (30 min, no Fe(II) present)	46,387	13,601 (267)	29 (1)	31,584 (638)	68 (1)	724 (26)	2 (0)	45,909 (931)	99 (2)
	t = 1 d	46,264	64 (27)	0 (0)	44,117 (952)	95 (2)	882 (15)	2 (0)	45,036 (994)	97 (2)
	t = 7.65 d	47,073	2 (0)	0 (0)	41,865 (1,176)	89 (2)	1,604 (33)	3 (0)	43,472 (1,209)	92 (3)

Table S5. Extent of Fe(II)-catalyzed Fe atom exchange in magnetite, magnetite with sorbed As(V) and As(V)-coprecipitated magnetite. Experiments were conducted with 1 gL^{-1} magnetite in 50 mM MOPS at pH 7.2.

		Aqueous Fe(II)					**Residual Solid**					TOTAL	
	Time (day)	Fe(II) (µmol)	% ^{57}Fe	% ^{54}Fe	% Ex. (^{57}Fe)	% Ex. (^{54}Fe)	Fe (µmol)	% ^{57}Fe	% ^{54}Fe	% Ex. (^{57}Fe)	% Ex. (^{54}Fe)	% Fe Recovery	pH
No As(V)	0	14.5 (0.2)	90.4 (1)	0.5 (0.1)	0 (0.1)	0 (0.1)	213 (23)	2.4 (0.1)	5.1 (0.1)	0 (0.1)	0 (1.2)	109 (11)	---
	0.01	14.5 (0.3)	62.6 (11.3)	1.9 (0.6)	3.9 (2.4)	3.4 (2.2)	184 (54)	4.6 (0.4)	4.9 (0.1)	4 (1.6)	5.8 (4.2)	95 (26)	7.27 (0.03)
	4.78	12.7 (0.4)	40.3 (5.3)	3 (0.2)	10.5 (2.4)	9.2 (1.8)	204 (31)	6.6 (0.2)	4.7 (0.1)	11.4 (1.5)	16.6 (5.8)	104 (15)	7.15 (0.05)
	6.91	12.7 (1.5)	42.7 (5.5)	2.9 (0.3)	9.4 (2.5)	8.6 (2.5)	228 (27)	6.5 (0.3)	4.7 (0)	10.6 (2.3)	15.6 (2.4)	115 (12)	7.16 (0.04)
As(V) Ads 13.3 µM	0	14.2 (0.4)	82.7 (1.9)	1.1 (0.07)	0 (0.2)	0 (0.1)	213 (23)	2.4 (0.1)	5.1 (0.1)	0 (0.1)	0 (1.4)	109 (11)	---
	0.01	19.6 (2.9)	46.9 (6.8)	2.8 (0.3)	6.5 (2.4)	5.8 (1.9)	178 (3)	4.6 (0.2)	5.1 (0.1)	5.2 (0.4)	-0.8 (3.5)	94 (1)	7.14 (0.11)
	4.77	15.3 (0.5)	40.2 (2.2)	3.1 (0.1)	8.7 (1)	8.3 (0.8)	187 (2)	6.3 (0.4)	4.8 (0.2)	10.3 (1.2)	12.1 (8.7)	97 (1)	7.17 (0.02)
	6.91	14.8 (0.3)	37.1 (1.7)	3.3 (0.1)	10.2 (0.9)	9.9 (0.6)	183 (9)	6.9 (0)	4.9 (0)	13 (0.6)	8 (2.2)	95 (4)	7.17 (0.05)
As(V) Ads 100 µM	0	14.6 (0.4)	90.8 (1)	0.3 (0)	0 (0.1)	0 (0.1)	213 (23)	5.1 (0.1)	5.1 (0.1)	2.6 (0)	0 (1.2)	109 (11)	---
	0.01	14.5 (0.3)	67 (3)	1.6 (0.2)	2.9 (0.6)	2.9 (0.6)	194 (12)	3.9 (0)	4.8 (0.1)	5.9 (0.3)	7.7 (2.3)	100 (6)	7.25 (0.01)
	4.77	14.2 (0.3)	47.2 (6.5)	2.6 (0.4)	7.8 (2.3)	7.1 (2.6)	187 (8)	5.6 (0.1)	4.7 (0)	12.1 (1.6)	14.4 (2.4)	97 (4)	7.17 (0.01)
	6.95	13.4 (0.5)	46.2 (5.7)	2.6 (0.3)	8 (2.2)	7.2 (1.9)	185 (30)	5.4 (0.2)	4.7 (0)	11.9 (2)	14.8 (2.2)	95 (15)	7.18 (0.02)
As(V) Ads 200 µM	0	17 (1.6)	87.3 (2)	0.5 (0.1)	0 (0.2)	0 (0.1)	213 (23)	5.1 (0.1)	5.1 (0.1)	2.7 (0.1)	0 (1.3)	110 (12)	---
	0.01	14.2 (0.1)	70 (3.9)	1.5 (0.2)	2.1 (0.6)	2 (0.5)	210 (9)	3.7 (0.1)	4.7 (0)	5.3 (0.3)	8.9 (0.6)	107 (4)	7.17 (0.01)
	5.04	13 (0.2)	60.6 (1.6)	1.9 (0.1)	3.6 (0.3)	3.5 (0.5)	177 (11)	5.2 (0.4)	4.7 (0)	8.5 (0.9)	12.1 (0.8)	91 (5)	7.14 (0.02)
	6.82	12.6 (0.2)	57.4 (3.1)	2.1 (0.2)	4.2 (0.7)	4.1 (0.7)	191 (14)	5.3 (0.1)	4.7 (0)	9.2 (0.6)	12.6 (1.5)	98 (7)	7.16 (0.02)
As(V) Coppt As:Fe = 0.0005	0	15.6 (0.2)	76 (7.1)	1.2 (0.34)	0 (0.8)	0 (0.7)	190 (16)	2.4 (0)	4.9 (0.0)	0 (0)	0 (0.3)	98 (8)	---
	0.01	18.7 (0.4)	32.1	3.4	11.4	11.2	1967 (16)	6.6 (0.2)	4.7 (0.0)	14.6 (1.1)	13.9 (3.3)	103 (7)	7.16 (0.02)
	5.33	12.6 (0.6)	27.1 (2.4)	3.6 (0.12)	15.4 (2.3)	15 (2.2)	189 (2)	8.7 (0.6)	4.6 (0.0)	26 (3.4)	24.4 (1.4)	96 (1)	7.14 (0.03)
	7.82	13.1 (0.5)	28.8 (2.7)	3.6 (0.14)	13.9 (2.1)	13.7 (2.2)	177 (3)	9 (0.1)	4.6 (0.1)	25.3 (2.1)	26.1 (5.9)	91 (1)	7.10 (0.01)
As(V) Coppt As:Fe = 0.0099	0	15.8 (0.2)	94.1 (1.1)	0.2 (0.1)	0 (0.1)	0 (0.1)	183 (41)	4.8 (0)	0 (0)	0 (0)	0 (0.6)	95 (20)	---
	0.01	13.5 (0.9)	75.3 (2.2)	1.2 (0.1)	2 (0.3)	2.1 (0.3)	183 (15)	4.8 (0.1)	3.7 (0.1)	3.7 (0.1)	3.6 (0.9)	94 (7)	7.16 (0.03)
	5.07	5.3 (0.3)	30 (2.8)	3.5 (0.2)	17.9 (2.6)	19.2 (3.2)	183 (32)	9 (0.5)	24.7 (0.8)	24.7 (0.8)	24.7 (2.9)	90 (15)	7.04 (0.01)
	6.97	5.1 (0.2)	32.1 (5.5)	3.4 (0.3)	16.6 (4.6)	17.2 (4.8)	166 (32)	9.7 (0.9)	25.4 (1.8)	25.4 (1.8)	24.2 (3.4)	82 (15)	7.03 (0.01)

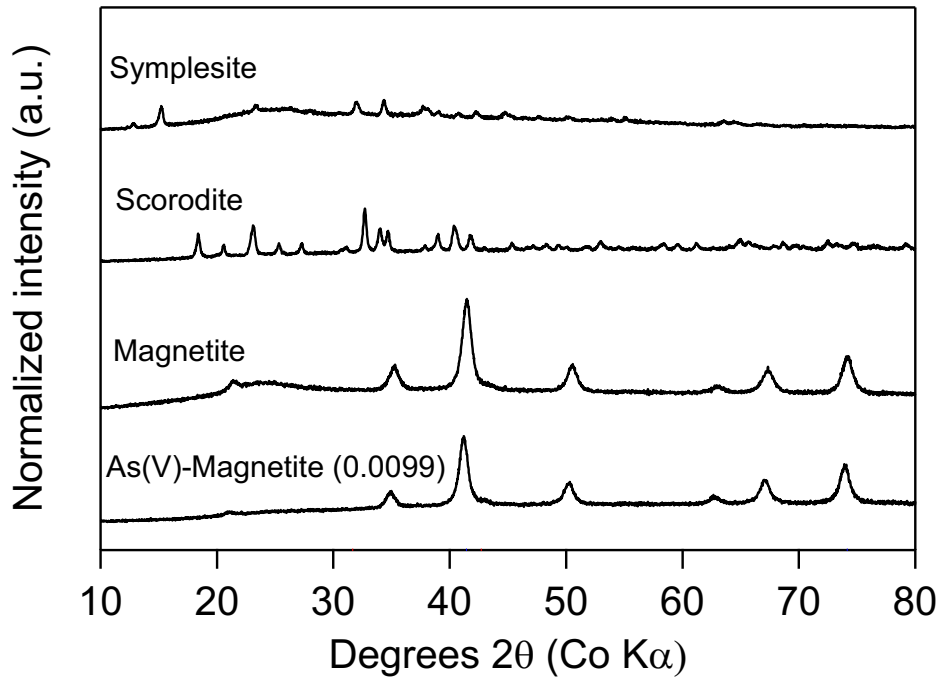

Figure S1. Powder X-ray diffraction pattern of the magnetite and As(V)-magnetite coprecipitate used in this study as compared with patterns for symplesite ($Fe^{II}_3(AsO_4)_2 \bullet 8(H_2O)$) and scorodite ($Fe^{III}AsO_4 \bullet 2(H_2O)$).

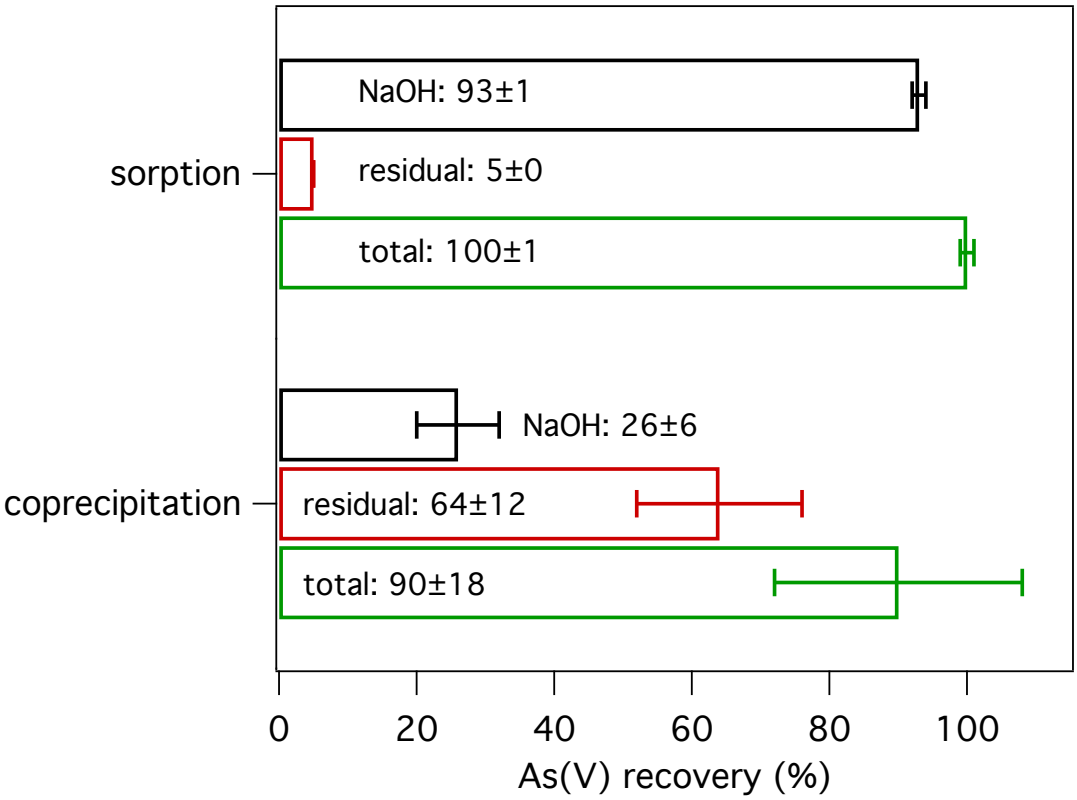

Figure S2. As recovered from magnetite with sorbed As(V) and As(V)-magnetite coprecipitates in the NaOH extraction step and subsequent total dissolution. In both experiments, the molar As:Fe ratio was 0.0099 and the overall total As recovery was ≥90%.

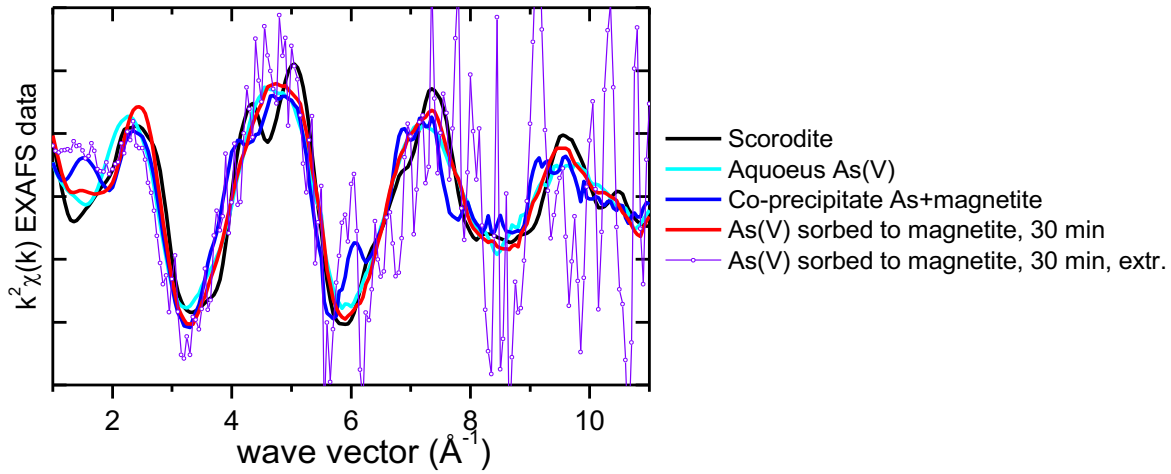

Figure S3. As K-edge EXAFS data of As(V) sorbed to magnetite for 30 min before (red line) and after (purple symbols) extraction with NaOH. The small fraction of As(V) remaining on the NaOH-extracted solids is responsible for the low signal-to-noise ratio of the measured spectrum, which impairs further structural analysis. Qualitative comparisons in the lower-noise region at low *k* suggests similarity to the co-precipitate sample (blue line), particularly around 1.8 $Å^{-1}$ and 6 $Å^{-1}$.

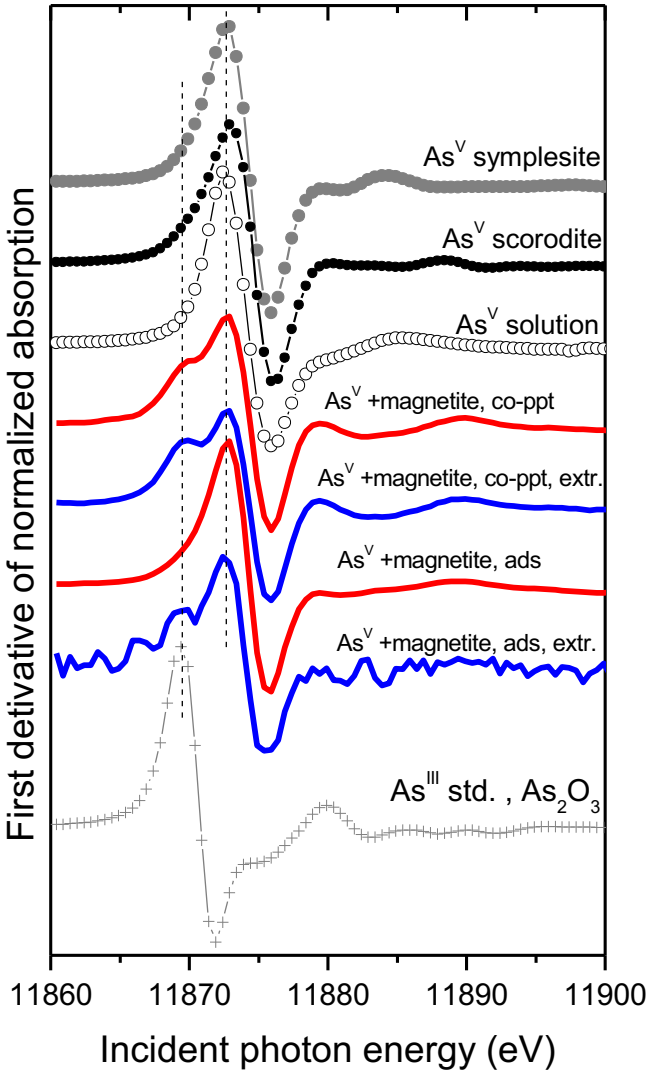

Figure S4. First derivative of the normalized absorption spectra from samples and standards. Magnetite with sorbed As(V) and As(V)-magnetite coprecipitate (As:Fe mole ratio of 0.007) samples are shown before and after extraction with NaOH. The vertical dashed lines indicate spectral features that correspond to the As(III) and As(V) standards.

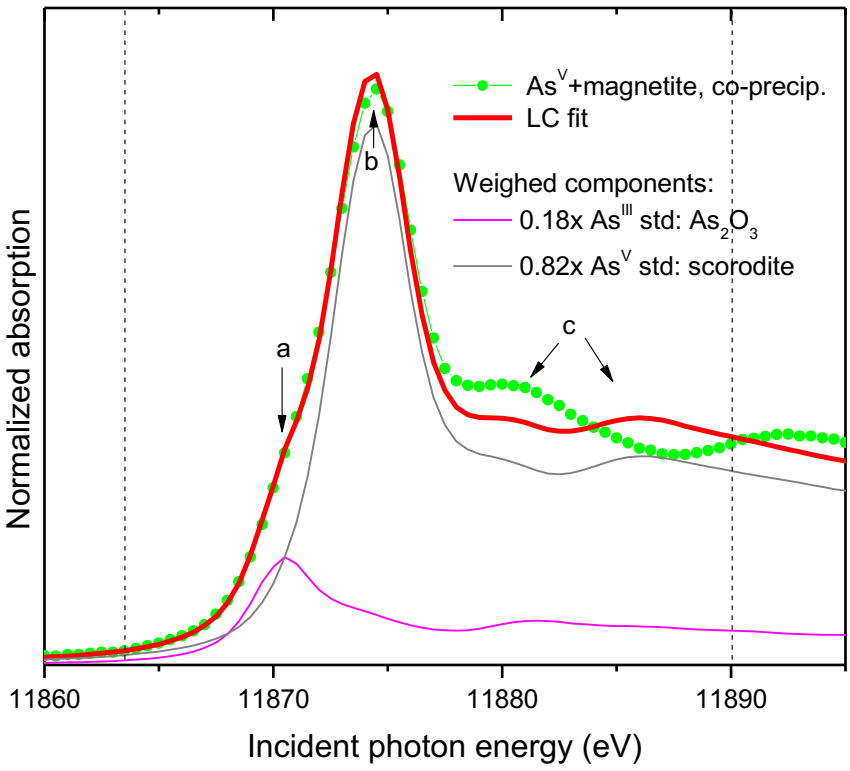

Figure S5. Linear combination (LC) fit of the XANES data from the As(V)-magnetite co-precipitation sample with As(III) and As(V) standards (data: green symbols, fit: red line). The fit range is shown by the dashed lines. The weighed contributions in the LC fit from the As(III) standard (magenta), and the As(V) standard (grey) are shown. The ~18% contribution from the As(III) standard is able to reproduce the shoulder at the edge position (arrow a) and the white line amplitude suppression (arrow b). The inability of the LC fit to reproduce the features indicated by arrow c is due to the different atomic coordination of As in the co-precipitation sample relative to the scorodite standard used here as a valence state reference.

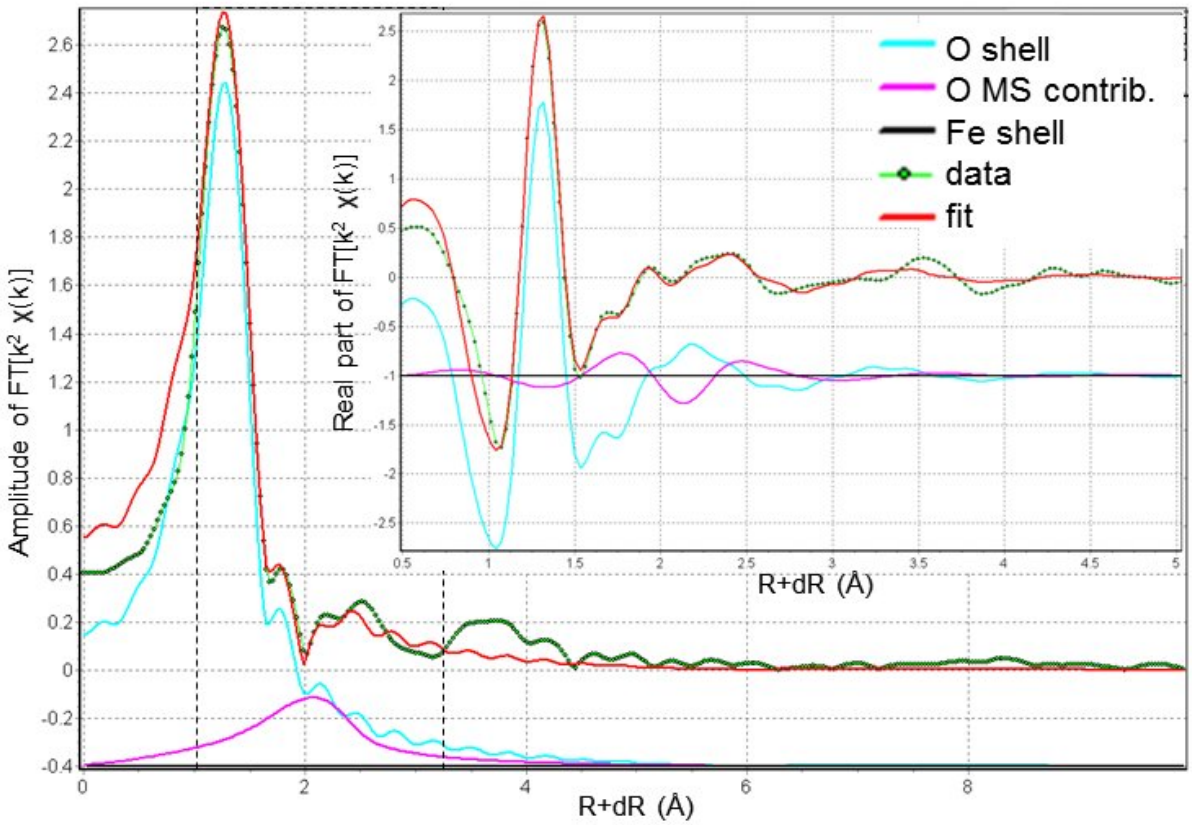

Figure S6a. Illustration of the fit quality for the EXAFS data from the aqueous As(V) standard. Main figure: magnitude of the Fourier Transform (FT), inset: real part of FT. The FT is over Δk = 2.8 - 12.1 $Å^{-1}$ with 1.0 $Å^{-1}$ wide Hanning window sills. The data are in green symbols, the fit is the red lines. The fit range is shown by the dotted lines. The contribution from the O shell (cyan) and the MS contribution within the AsO_4 tetrahedron (magenta) are also shown. Note that the individual contributions combine linearly to produce the fit line only in the real part of the FT. The numerical values and the constraints used in the fit are listed in Table 2.

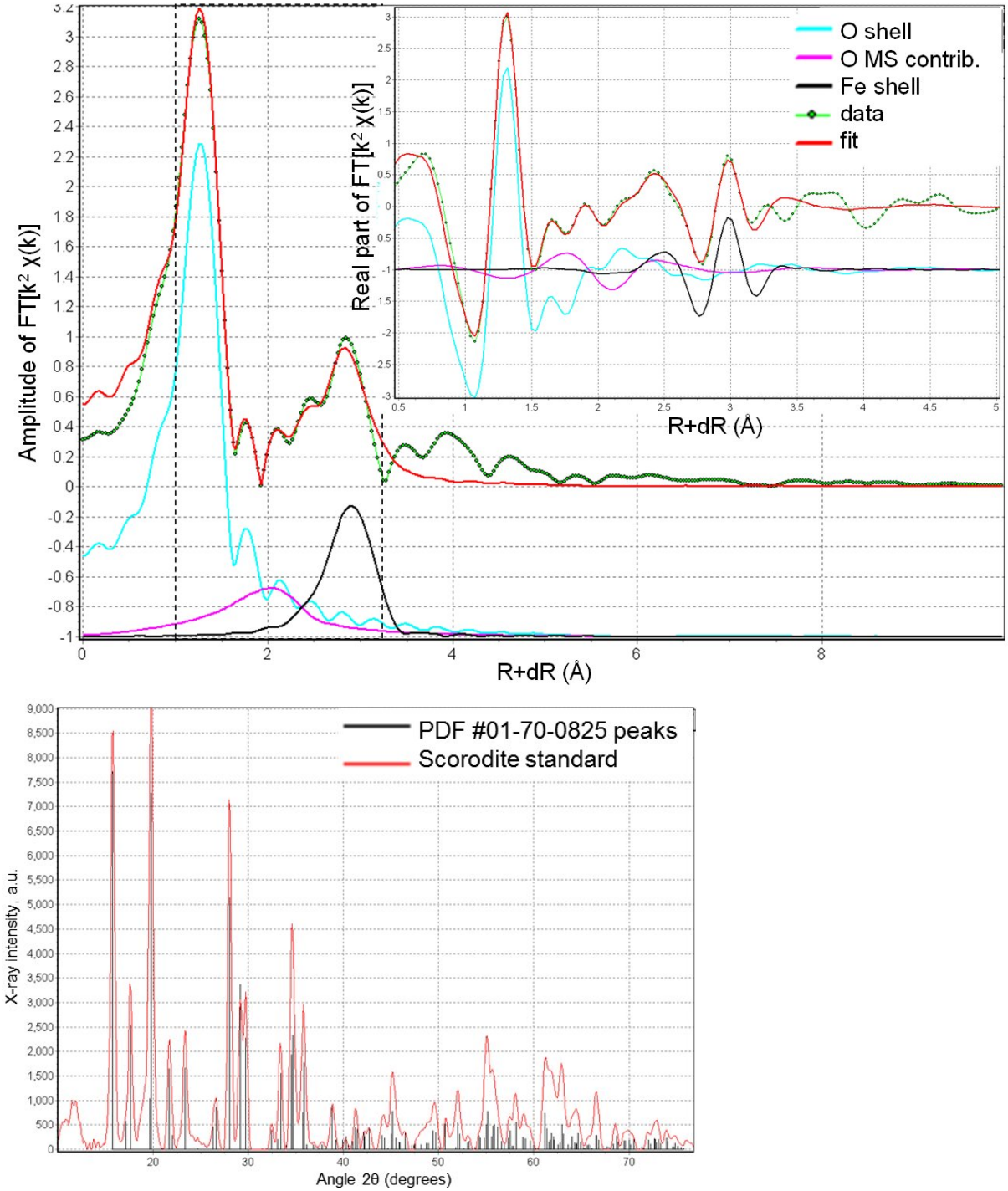

Figure S6b. Illustration of the fit for the EXAFS data from the scorodite standard. Main figure: magnitude of the Fourier Transform (FT), inset: real part of FT. The FT is over $\Delta k = 2.8 = 12.1$ Å^{-1} with 1.0 Å^{-1} wide Hanning window sills. The data are in green symbols, the fit is the red lines. The fit range is shown by the dotted line. The numerical values and the constraints used in the fit are listed in Table 2. The powder XRD pattern verifying that the standard is scorodite is shown at the bottom.

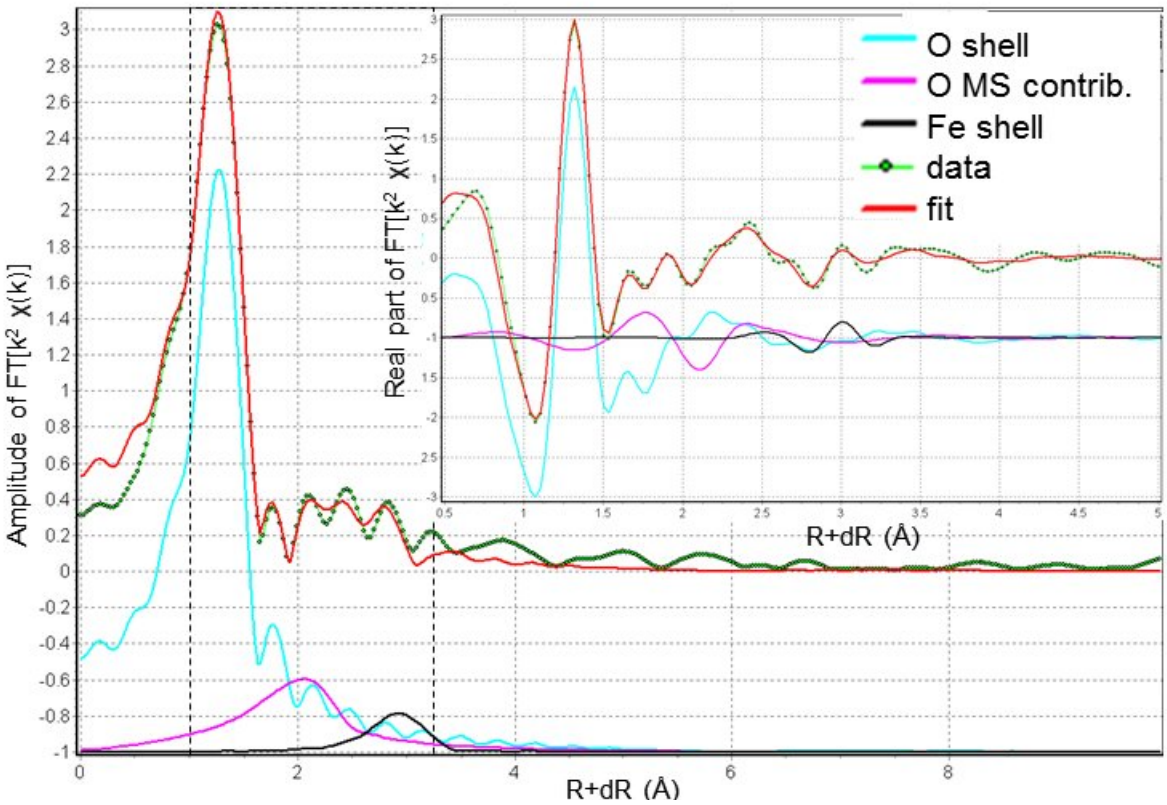

Figure S6c. Illustration of the fit quality for the EXAFS data from the As(V) + magnetite, adsorption, 30 min sample. Main figure: magnitude of the Fourier Transform (FT), inset: real part of FT. The FT is over Δk = 2.8 - 12.1 $Å^{-1}$ with 1.0 $Å^{-1}$ wide Hanning window sills. The data are in green symbols, the fit is the red lines. The fit range is shown by the dotted lines. The individual contributions from the O shell (cyan), the MS paths within the AsO_4 tetrahedron (magenta), and the Fe shell (black) are also shown. The numerical values and the constraints used in the fit are listed in Table 2.

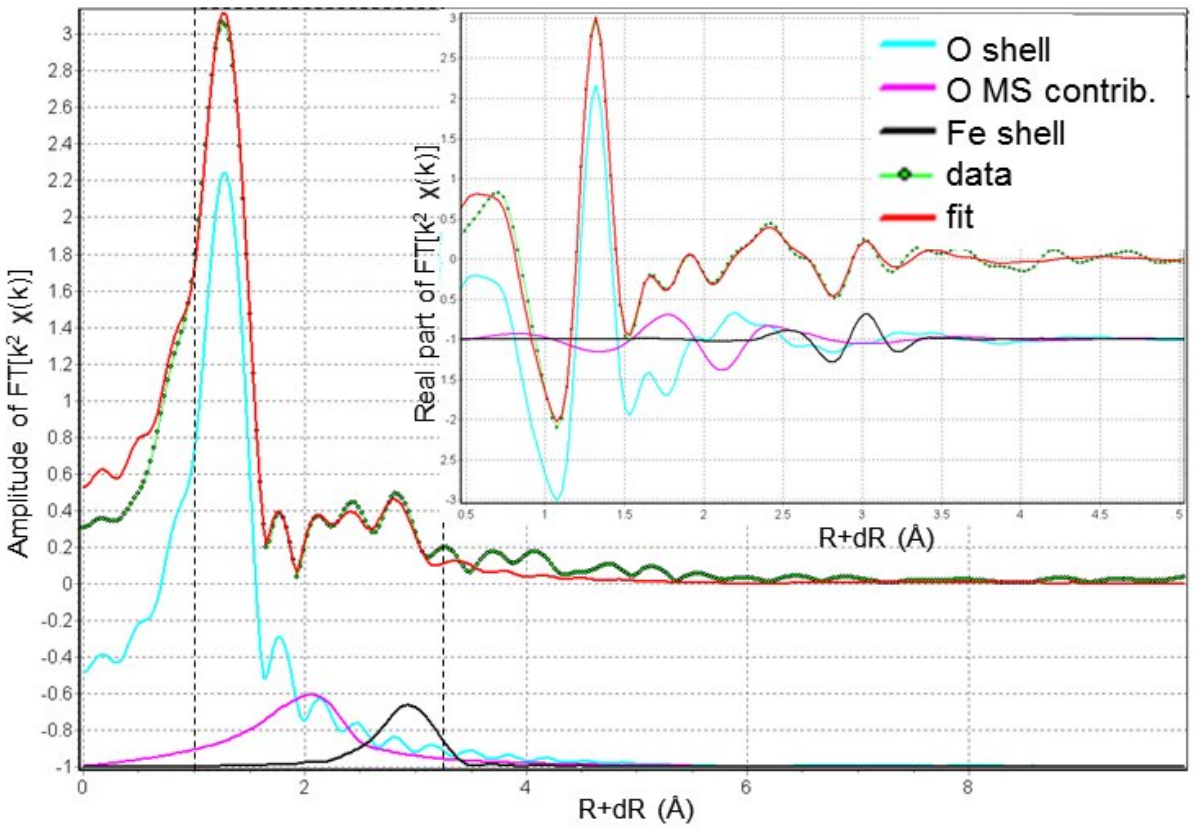

Figure S6d. Illustration of the fit quality for the EXAFS data from the As(V) + magnetite, adsorption, 3.5 d sample. Main figure: magnitude of the Fourier Transform (FT), inset: real part of FT. The FT is over $\Delta k = 2.8 - 12.1$ Å^{-1} with 1.0 Å-1 wide Hanning window sills. The data are in green symbols, the fit is the red lines. The fit range is shown by the dotted lines. The individual contributions from the O shell (cyan), the MS paths within the AsO_4 tetrahedron (magenta), and the Fe shell (black) are also shown. The numerical values and the constraints used in the fit are listed in Table 2.

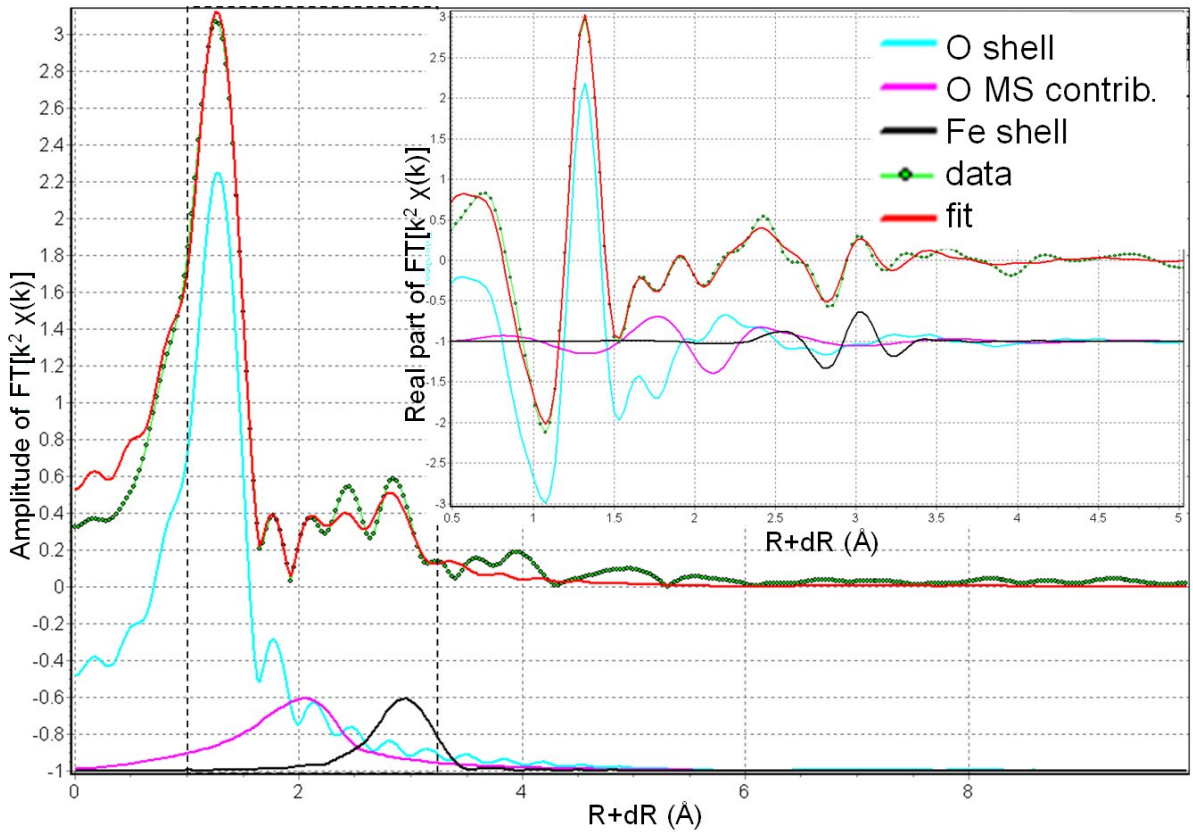

Figure S6e. Illustration of the fit quality for the EXAFS data from the As(V) + magnetite, adsorption, 4 weeks sample. Main figure: magnitude of the Fourier Transform (FT), inset: real part of FT. The FT is over Δk = 2.8 - 12.1 $Å^{-1}$ with 1.0 $Å^{-1}$ wide Hanning window sills. The data are in green symbols, the fit is the red lines. The fit range is shown by the dotted lines. The individual contributions from the O shell (cyan), the MS paths within the AsO_4 tetrahedron (magenta), and the Fe shell (black) are also shown. The numerical values and the constraints used in the fit are listed in Table 2.

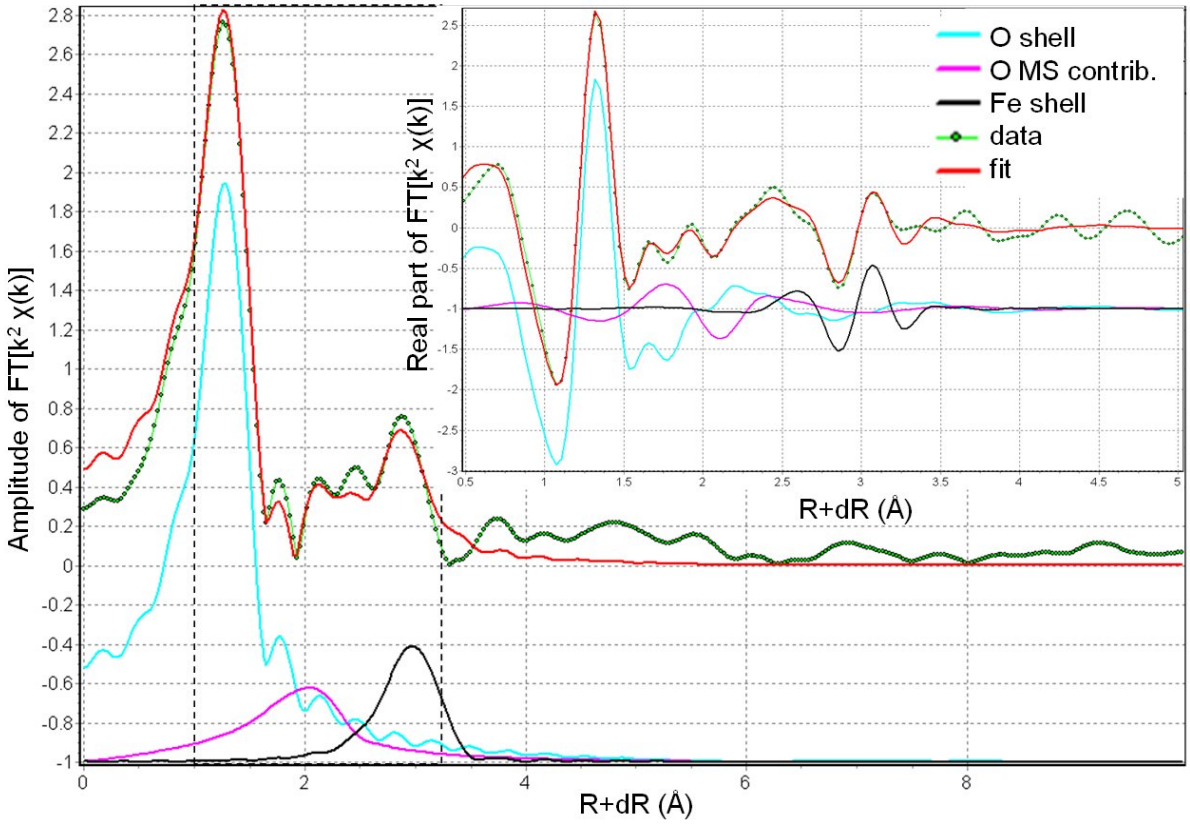

Figure S6f. Illustration of the fit quality for the EXAFS data from the As(V) + magnetite, co-precipitation sample. Main figure: magnitude of the Fourier Transform (FT), inset: real part of FT. The FT is over Δk = 2.8 - 12.1 $Å^{-1}$ with 1.0 $Å^{-1}$ wide Hanning window sills. The data are in green symbols, the fit is the red lines. The fit range is shown by the dotted lines. The individual contributions from the O shell (cyan), the MS paths within the AsO_4 tetrahedron (magenta), and the Fe shell (black) are also shown. The numerical values and the constraints used in the fit are listed in Table 2.

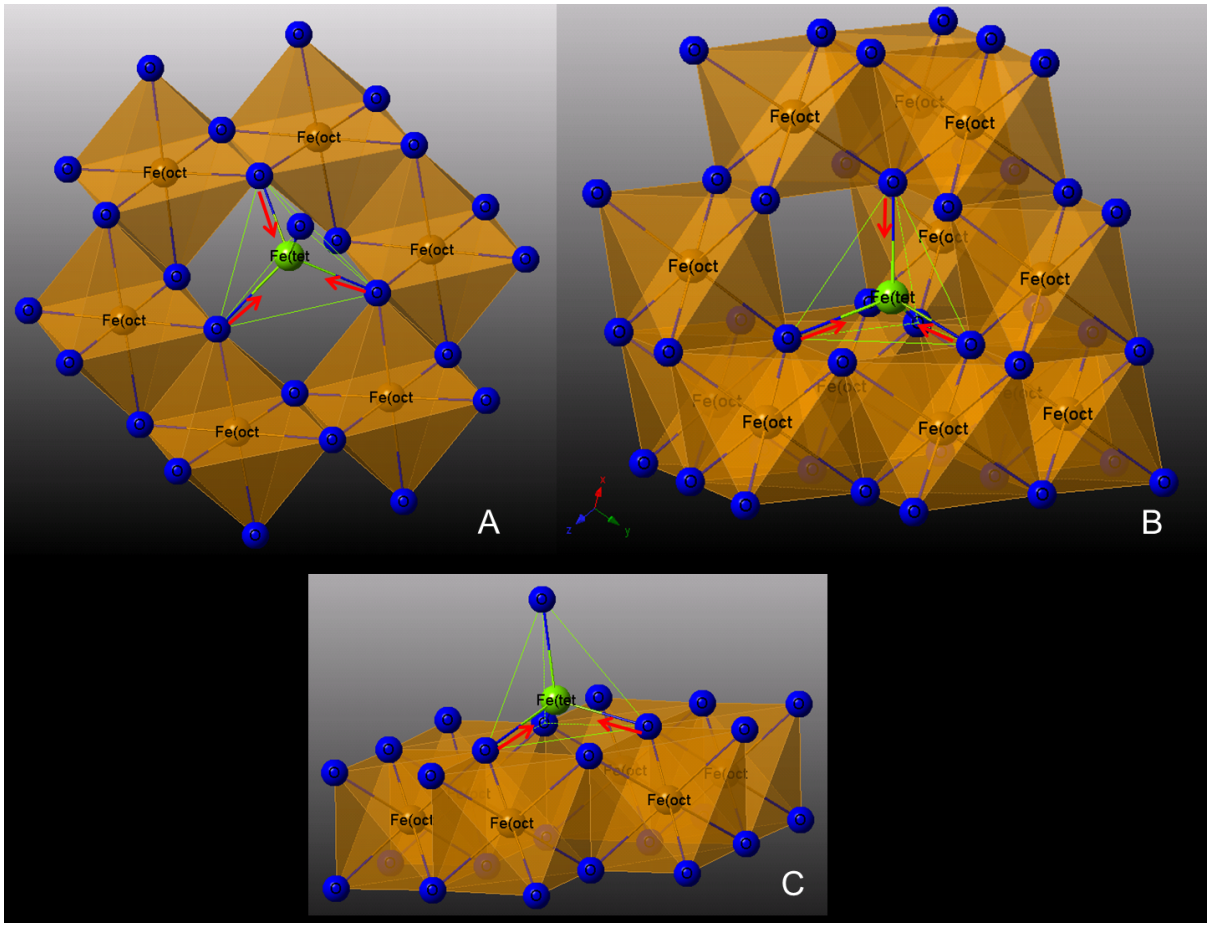

Figure S7. Arrangement of the Fe octahedra (orange) around the tetrahedral Fe site (green) in magnetite. Depiction based on the crystallographic data in Haavik et al. (reference 57 in the main text). The tetrahedral site occupies the space above the void in the octahedral (111) plane. The distortions required to fit the shorter-distance As(V) octahedron are show by red arrows. (A) View from above the (111) plane; (B) View along the (111) plane, with some octahedra above the plane shown; (C) View along the (111) plane, without additional Fe octahedral above the plane.

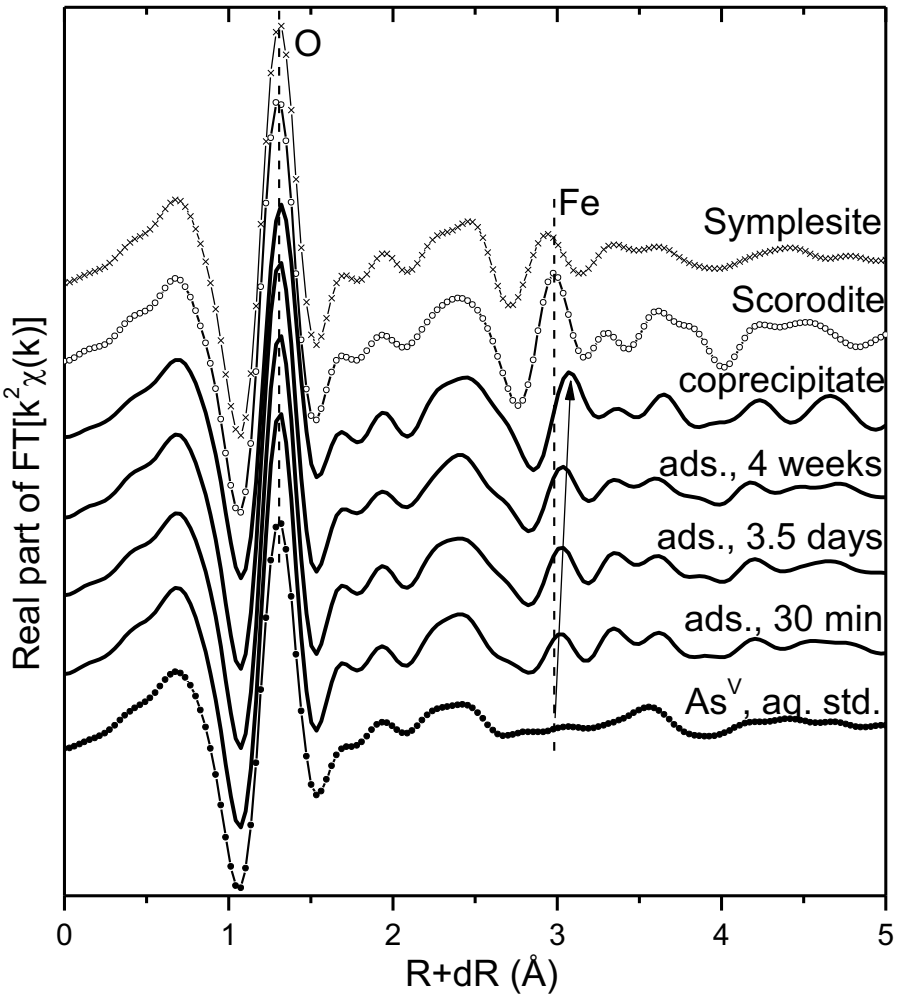

Figure S8. Fourier transform of the k^2-weighed As K-edge EXAFS data (real part) of sorbed As(V) and magnetite coprecipitated As(V) as well as As reference materials (aqueous As(V), Fe-As phases symplesite and scorodite). The vertical dashed lines indicate the features corresponding to the O and Fe coordination shells in scorodite. Experimental data presented as solid lines and standards as lines with symbols. The arrow indicates the increasing As-Fe distance in the sorption samples with reaction time.

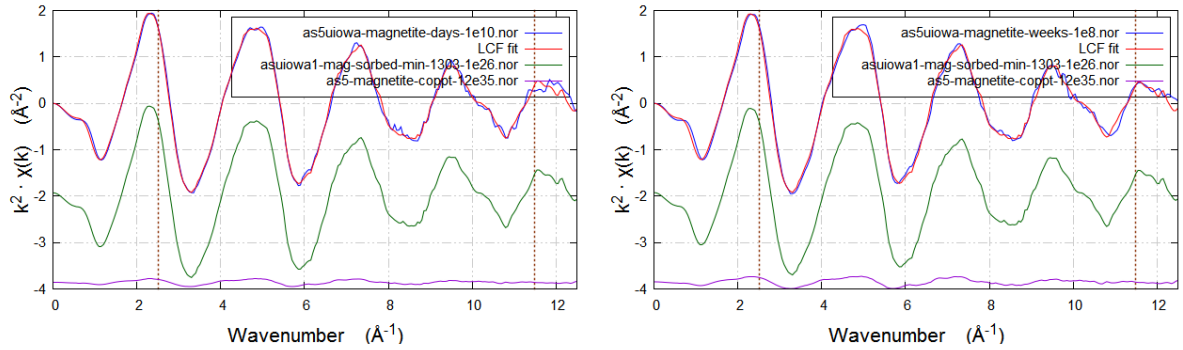

Figure S9. Linear combination (LC) fits of the EXAFS data from As(V) sorbed to magnetite after 3.5 d (left) and 28 d (right), using the adsorption and co-precipitation samples as endmembers. The data are shown in blue lines, the fit is shown in red lines. The fit range is indicated by the dotted lines. The weighed contributions in the LC fit from the 30 min adsorption sample (green), and the As(V)-magnetite co-precipitation sample (purple) are shown at the bottom. The refined proportions of the spectral endmembers are 5% co-precipitated standard for the 3.5 d sample and 8% co-precipitated standard for the 28 d sample, balance is the 30 min adsorption standard. These numerical values are discussed in the main text.

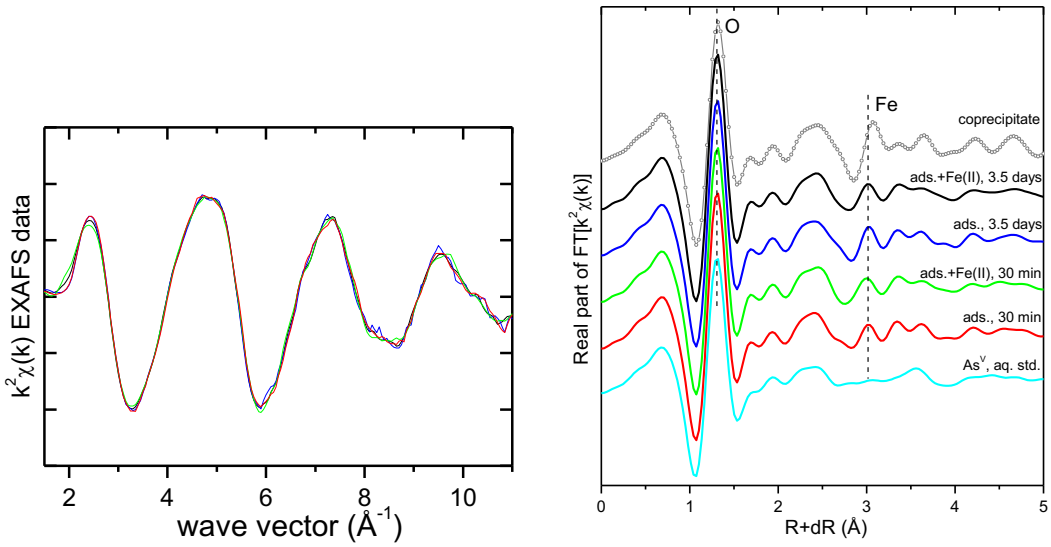

Figure S10: Left: Comparison of the k^2-weighed EXAFS spectra from As(V) adsorbed on magnetite with and without added Fe(II) for 30 min and 3.5 d, showing that the same data are obtained in all reactors. Right: Real part of the Fourier transformed EXAFS data from the left figure compared to the aqueous As(V) standard and As(V) co-precipitated with magnetite. The spectra are offset vertically for clarity. The same color convention is used in both graphs.

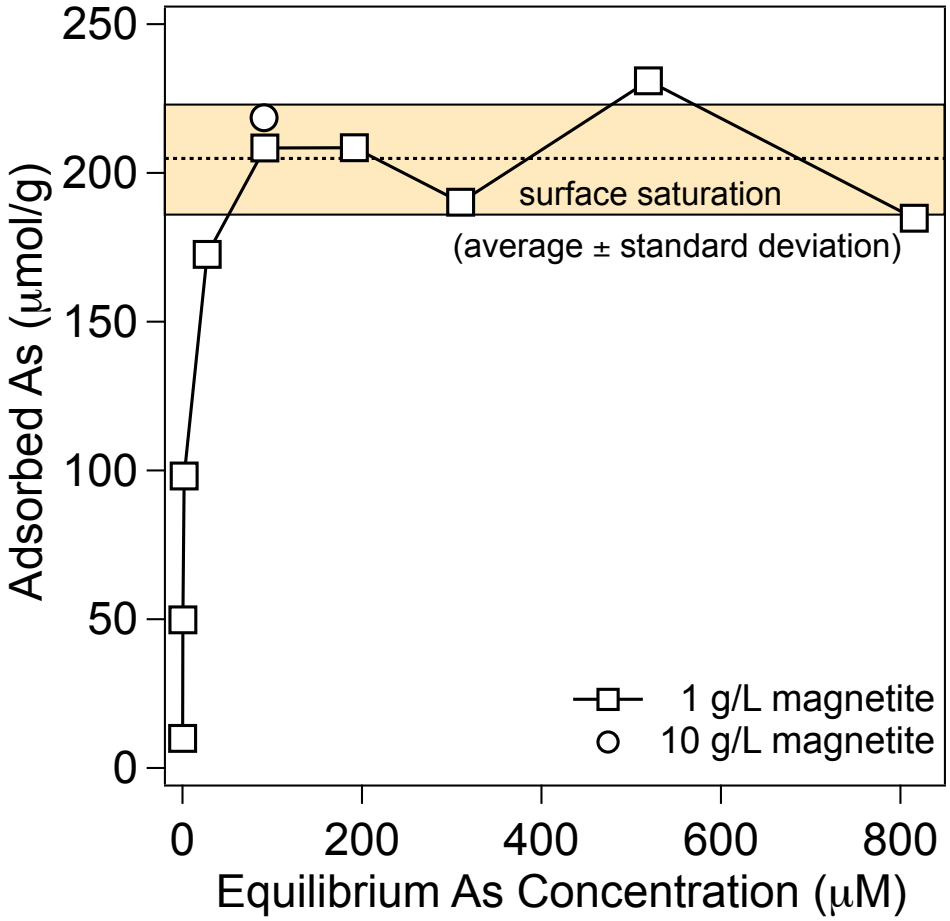

Figure S11. As(V) adsorption isotherm on magnetite (solids loading 1 g L^{-1}) buffered at pH 7.2 with 50 mM MOPS. Data from XAS reactors (10 g/L, 3092 μM initial As(V) concentration; from Table S4) was re-calculated to match the same solids loading by dividing the equilibrium aqueous As concentration by 10 (ratio of mass loadings).

References

1. Frierdich AJ, Helgeson M, Liu C, Wang C, Rosso KM, Scherer MM. Iron Atom Exchange between Hematite and Aqueous Fe(II). Environ Sci Technol. 2015;49(14):8479-86.
2. Gorski CA, Handler RM, Beard BL, Pasakarnis T, Johnson CM, Scherer MM. Fe Atom Exchange between Aqueous Fe^{2+} and Magnetite. Environ Sci Technol. 2012;46:12399-407.
3. Handler RM, Frierdich AJ, Johnson CM, Rosso KM, Beard BL, Wang C, Latta DE, Neumann A, Pasakarnis T, Premaratne WAPJ, Scherer MM. Fe(II)-Catalyzed Recrystallization of Goethite Revisited. Environ Sci Technol. 2014;48(19):11302-11.
4. Latta DE, Bachman JE, Scherer MM. Fe Electron Transfer and Atom Exchange in Goethite: Influence of Al-Substitution and Anion Sorption. 2012.
5. Mikutta C, Wiederhold JG, Cirpka OA, Hofstetter TB, Bourdon B, von Gunten U. Iron isotope fractionation and atom exchange during sorption of ferrous iron to mineral surfaces. Geochim Cosmochim Acta. 2009;73:1795-812.